HHS Public Access

Author manuscript

Cell Metab. Author manuscript; available in PMC 2024 October 03.

Published in final edited form as:

Cell Metab. 2023 October 03; 35(10): 1767–1781.e6. doi:10.1016/j.cmet.2023.09.001.

KETOGENESIS PROMOTES TOLERANCE TO *PSEUDOMONAS AERUGINOSA* PULMONARY INFECTION

Kira L. Tomlinson[1], **Ying-Tsun Chen**[1], **Alex Junker**[1], **AndreaCarola Urso**[1], **Tania Wong Fok Lung**[1], **Danielle Ahn**[1], **Casey E. Hofstaedter**[2], **Swikrity U. Baskota**[3], **Robert K. Ernst**[2], **Alice Prince**[1], **Sebastián A. Riquelme**[1,*]

[1]Department of Pediatrics, Columbia University, New York, NY 10032, USA

[2]Department of Microbial Pathogenesis, University of Maryland, Baltimore, MD 21201, USA

[3]Department of Pathology and Cell Biology, Columbia University, New York, NY 10032, USA

SUMMARY

Pseudomonas aeruginosa is a common cause of pulmonary infection. As a Gram-negative pathogen, it can initiate a brisk and highly destructive inflammatory response; however, most hosts become tolerant to the bacterial burden, developing chronic infection. Using a murine model of pneumonia, we demonstrate that this shift from inflammation to disease tolerance is promoted by ketogenesis. In response to pulmonary infection ketone bodies are generated in the liver and circulate to the lungs where they impose selection for *P. aeruginosa* strains unable to display surface lipopolysaccharide (LPS). Such keto-adapted LPS strains fail to activate glycolysis and tissue damaging cytokines and, instead, facilitate mitochondrial catabolism of fats and oxidative phosphorylation (OXPHOS), which maintains airway homeostasis. Within the lung, *P. aeruginosa* exploits the host immunometabolite itaconate to further stimulate ketogenesis. This environment enables host-*P. aeruginosa* coexistence, supporting both pathoadaptive changes in the bacteria and the maintenance of respiratory integrity via OXPHOS.

Graphical Abstract

*Lead Contact: Sebastián A. Riquelme, sr3302@cumc.columbia.edu.

Author contributions

Conceptualization, K.L.T., S.A.R.; Methodology, K.L.T., S.A.R.; Software, K.L.T., S.A.R.; Validation, K.L.T., S.A.R; Formal Analysis, K.L.T., Y.C., S.U.B., C.E.H., S.A.R; Investigation, K.L.T., Y.C., A.J., A.U., D.A., T.W.F.L., S.U.B., C.E.H., R.K.E., S.A.R.; Resources, S.A.R., R.K.E., A.P.; Data Curation, K.L.T., S.A.R., Writing – original draft, K.L.T., S.A.R., Writing – Review & Editing, K.L.T., A.P., S.A.R.; Visualization, K.L.T., S.A.R.; Supervision, S.A.R, A.P.; Project Administration, K.L.T., S.A.R., Funding Acquisition, S.A.R. and A.P.

Declaration of interests

The authors declare no competing interests.

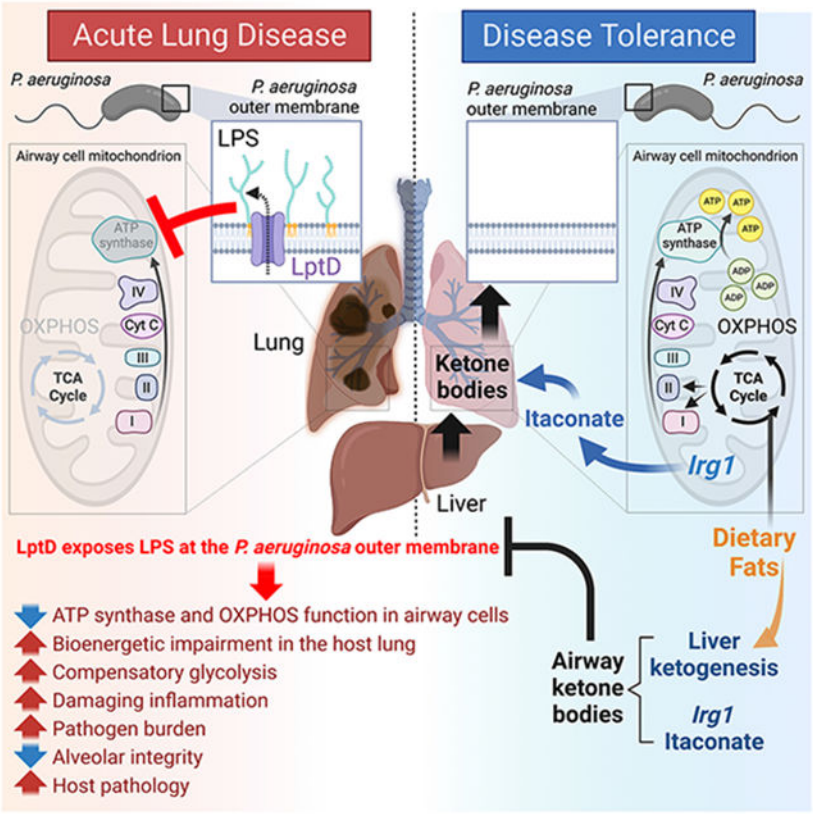

eTOC blurb

Tomlinson et al report how ketogenesis, a metabolic response to host energy deprivation, promotes disease tolerance during *P. aeruginosa* pneumonia. Ketone bodies select *P. aeruginosa* strains unable to assembly surface LPS, preserving thus the ability of infected airway cells to produce ATP in mitochondria. This favorable microenvironment facilitates host-pathogen coexistence.

INTRODUCTION

Pseudomonas aeruginosa is a feared pulmonary pathogen associated with acute, inflammatory infection resulting in substantial lung destruction caused by its expression of potent toxins and proteases[1]. More commonly, however, it is associated with persistent infection in people with cystic fibrosis (CF)[2,3], bronchiectasis[4,5], chronic obstructive pulmonary disease[6,7] and primary ciliary dyskinesia[8,9], subjects without underlying immune dysfunction. These patients develop tolerance to infection, also known as disease tolerance, an evolutionarily conserved defense strategy that controls damage in infected tissues by limiting the inflammatory response against the infectious agent[10-12]. By reducing inflammation, tolerance to infection not only preserves organ function, but also enables pathogen coexistence with the host[10-12]. Exactly how the host shifts from an immune response that is highly damaging to one that tolerates bacterial burden in the airway is not well understood.

The physiological processes that normally maintain pulmonary homeostasis are predominantly sustained by oxidative phosphorylation (OXPHOS)[13-15]. OXPHOS produces ATP in mitochondria, a process fueled by fats that are normally assimilated from the diet[16,17]. The energy provided by OXPHOS not only supports airway cell viability, but also promote numerous processes essential for normal pulmonary function, such as gas exchange, airway mucus clearance, and surfactant production[18-22]. In response to an infectious threat, including lipopolysaccharide (LPS) displayed by Gram-negative pathogens like *P. aeruginosa*, there is a rapid shift from these basal biological activities supported by OXPHOS to glycolysis[16,17,23-25]. This metabolic reprogramming generates inflammatory cytokines to eradicate infection[23,25]. This acute inflammation compromises the integrity of the lung and can be fatal if not regulated[1,10,11,26,27]. However, LPS not only drives local bioenergetic alterations, but also systemic host adaptations like ketogenesis[28,29]. By prompting ketogenesis, hepatic cells redirect fatty acids to produce ketone bodies, which travel to affected organs to stimulate ATP synthesis via OXPHOS[29,30]. By refueling ATP generation, ketone bodies impede tissue necrosis, phagocyte activation, and inflammation[29]. Hosts tolerant of pulmonary infection thus must tightly control the balance between OXPHOS, glycolysis, ketogenesis, and inflammation to safeguard lung integrity.

Bacteria also must adapt to the bioenergetic configuration of the airway. Clinical isolates of *P. aeruginosa* from the lung of tolerant subjects exhibit numerous LPS alterations[3,31], especially inactivating *lptD* mutations[32]. LptD is a key transporter that enables the display of LPS on the outer membrane of the bacterial surface, and is thus essential for its pro-inflammatory activity[33,34]. Along with changes in cell surface structures, these pathogens readily adapt their own metabolic activity to contribute to the preservation of the local environment[3,35]. In such a favorable milieu, *P. aeruginosa* evolves to persist as discrete communities that engraft within the local microbiome[2-7,36,37]. Adaptive changes observed in *P. aeruginosa* strains from chronically infected patients must synchronize with the bioenergetic setting that conserves pulmonary integrity: OXPHOS.

Here, we establish that tolerance to *P. aeruginosa* lung infection is closely associated with the maintenance of OXPHOS in airway cells. We demonstrate that the infected, tolerant host abrogates glycolysis and the release of airway-damaging cytokines by fueling pulmonary OXPHOS with fat metabolism. Ketogenesis and local immunometabolites in turn drive the selection of *P. aeruginosa* strains with limited display of LPS and enhanced ability to sustain the tolerogenic environment. This milieu not only safeguards respiratory integrity, but also promotes pathogen survival, enabling host-*P. aeruginosa* coexistence, which is hallmark of tolerance to infection.

RESULTS

P. aeruginosa surface LPS drives airway OXPHOS impairment via depletion of ATP synthase –

Using a LptD mutant of the laboratory *P. aeruginosa* strain PAO1 unable to display LPS on the surface (*ΔlptD* PAO1)[32,38], we demonstrated that LPS anchored to the outer membrane induces pulmonary OXPHOS dysfunction. In contrast with mice exposed to *ΔlptD* PAO1 (~10^6 CFUs; Fig. S1A), lung protein extracts from animals infected with WT PAO1

exhibited depletion of ATP5A, a key component of ATP synthase (also known as complex V), the OXPHOS machinery that generates ATP[39] (Fig. 1A). We did not observe substantial changes in other mitochondrial complexes involved in OXPHOS, including Sdhb (complex II: succinate dehydrogenase) and Mtco1 (complex IV: cytochrome C oxidase)[40,41] (Fig. 1A). As expected, depletion of ATP synthase in response to *P. aeruginosa* surface LPS correlated with activation of compensatory routes like glycolysis, illustrated by augmented expression of the pro-glycolytic enzyme hexokinase 2 (HK2)[42] (Fig. 1A) and increased glucose concentration in bronchoalveolar lavage (BAL) fluids (Fig. 1B).

We found that *P. aeruginosa* surface LPS provoked pulmonary depletion of ATP synthase via pathogen burden. Compared to the *ΔlptD* mutant, the WT PAO1 strain more readily consumed the pro-ATP NADH and $FADH_2$ intermediates that are generated from succinate and its precursor α–ketoglutarate[43] (Fig. 1C). This increased bioenergetic efficiency augmented *P. aeruginosa* biomass generation in succinate (Fig. 1D). To amplify *ΔlptD* PAO1 loads in the host airway, we exposed mice to an increasing inoculum of this strain. At lower doses (e.g., ~10^5 CFUs), *ΔlptD* PAO1 did not provoke substantial depletion of the ATP synthase constituent ATP5A, but at higher inoculum (e.g., > ~10^6 CFUs) it did (Fig. 1E).

We confirmed these findings *in vitro.* Bone-marrow derived macrophages (BMDMs) were exposed to either PBS or a similar inoculum of either WT PAO1 or *ΔlptD* PAO1, and their OXPHOS response was analyzed via Seahorse technology. Compared to BMDMs administered *ΔlptD* PAO1, cells exposed to WT PAO1 had a higher oxygen consumption rate (OCR) (Fig. 1F), which is a signature of mitochondrial OXPHOS impairment by LPS stimulation[32,44,45] (Fig. 1G). However, when compared to BMDMs treated with PBS, cells exposed to either pathogen elicited significantly higher OCR throughout the course of the assay (Fig. 1F), supporting the idea that *P. aeruginosa* LptD causes host OXPHOS interference via both LPS display and bacterial burden.

P. aeruginosa inhibition of host ATP synthase triggers damaging inflammation –

We confirmed the damaging consequences of *P. aeruginosa* interference of host ATP synthase in a model of acute pneumonia. We treated animals with a sublethal dose of oligomycin (~0.2mg/Kg), which is a specific inhibitor of ATP synthase[46], prior to infection with ~10^5 CFUs of WT PAO1. Oligomycin amplified the accumulation of IL-1β and TNFα (Fig. 2A), cytokines associated with tissue damage, as well as increased WT PAO1 burden (Fig. 2B). To further demonstrate that blockade of host mitochondrial bioenergetics exacerbates lung inflammatory stress during infection, we blocked fatty acid β-oxidation (FAO), a pathway upstream of OXPHOS that fuels host ATP synthase activity[47]. FAO metabolizes fatty acids that are trafficked into mitochondria by the transporter *Cpt1a*[47]. These imported metabolites are then β-oxidized, generating intermediates that enter the TCA cycle to fuel OXPHOS and ATP synthase function. To interfere with host FAO, we treated mice with a specific *Cpt1a* blocker, etomoxir[48]. In contrast with controls, mice treated with etomoxir and infected with WT PAO1 had significantly higher levels of IL-6 and TNFα (Fig. 2C) and increased bacterial burden (Fig. 2D). Similar findings were observed in animals exposed to *ΔlptD* PAO1 (Fig. 2E-F), confirming that impairment of pathways that fuel host ATP synthase intensifies airway disease.

We observed that cytokines promoted by host ATP synthase interference triggered an inflammatory feedback loop that worsened pulmonary integrity. Compared to *Il1r*$^{-/-}$ mice, which are unable to signal through IL-1β, *Il1r*$^{+/+}$ animals exposed to WT PAO1 had significantly increased airway levels of IL-6 (~2.7 fold) and TNFα (~1.8 fold) (Fig. S1B), augmented bacterial burden in BAL (~27 fold) (Fig. S1C), and greater albumin leakage into the airway fluid (Fig. S1D), which is an indicator of vascular barrier damage[49,50]. These findings were further supported using WT and *ΔlptD* PAO1 strains (Fig. S1E-G).

P. aeruginosa strains from tolerant hosts preserve lung OXPHOS during pneumonia –

We next addressed whether clinical isolates of *P. aeruginosa* from tolerant subjects, in fact, maintain host OXPHOS and if this is linked to the repression of LptD. We found that ~85% of *P. aeruginosa* strains from the airways of 13 subjects in the intensive care unit (ICU) exhibited substantially lower mRNA expression of *lptD*, in contrast with WT PAO1 (Fig. 3A). Similar findings were observed with longitudinal collections of *P. aeruginosa* isolates from the lungs of two chronically infected individuals with CF (CF#1 and CF#2). Analysis of 14 *P. aeruginosa* strains from CF#1 showed that, at advanced stages of infection, 100% of these pathogens exhibited low *lptD* expression (Fig. 3B, left panel). We validated these observations by examining 17 *P. aeruginosa* strains from CF#2, which showed null *lptD* expression (Fig. 3B, right panel). These data confirmed the association between tolerance to *P. aeruginosa* infection and LptD inhibition.

We next analyzed how *P. aeruginosa* isolates from the lung of tolerant subjects affected pulmonary ATP synthase. Compared to animals exposed to WT PAO1, mice infected with a mixture of the 17 isolates from CF#2 (hereafter referred to as *"P. aeruginosa* isolates") (Fig. 3B, left panel; Fig. S1H) preserved ATP5A expression in the lung tissue (Fig. 3C). They did not trigger any changes in mitochondrial complexes II and IV, nor increased pro-inflammatory glycolytic metabolism via HK2 (Fig. 3C).

To better appreciate how the stress of bacterial infection impacts mitochondrial bioenergetics at the cellular level, we performed single-cell-RNA-sequencing (scRNA-Seq) of whole lung tissue from animals exposed to either PBS, WT PAO1, or the *P. aeruginosa* isolates. We were more specifically interested in delineating changes in bioenergetics in immune versus stromal cell populations. Initial clustering of our integrated scRNA-Seq data identified 23 populations with distinctive transcriptomic signatures, including cells in direct contact with the airway lumen, such as alveolar macrophages, type 1 and 2 pneumocytes, ciliated cells, fibroblasts, and vascular and capillary endothelial cells, as well as cells that are not directly exposed to the airway, such as mesothelial cells and smooth muscle cells (Fig. 3D, Fig. S1I-J, Table S1). We computed OXPHOS scores for every cell using 171 genes associated with the pathway, including ATP synthase and complexes I-IV in the electron transport chain (ETC) (Table S2)[51]. We then calculated a ΔOXPHOS score compared to uninfected, PBS-treated mice, and created volcano plots to visualize how the different *P. aeruginosa* strains affected this bioenergetic pathway in each cell cluster. As anticipated, WT PAO1, but not the *P. aeruginosa* isolates, significantly compromised OXPHOS in key respiratory cells. While WT PAO1 suppressed OXPHOS in 13 out of the 23 populations identified (~57%) (Fig. 3E), the *P. aeruginosa* isolates only caused OXPHOS downregulation in 5 (~22%) (Fig.

3F). One of the most highly impacted populations in WT PAO1-infected mice were alveolar macrophages, followed by cell populations required to maintain pulmonary gas exchange and surfactant production, including type 2 pneumocytes, vascular and capillary endothelial cells[13] (Fig. 3E). Conversely, the *P. aeruginosa* isolates did not compromise OXPHOS in these cell subsets (Fig. 3F). Instead, the *P. aeruginosa* isolates impaired OXPHOS in recruited phagocytes (~60% of cells affected), including peripheral blood (PB) neutrophils, granulocytes, and regulatory myeloid cells, indicating that the *P. aeruginosa* isolates preserve the bioenergetic homeostasis of resident respiratory cells.

Preservation of host ATP synthase function enables disease tolerance –

Our findings this far indicated that the host responded to infection by the *P. aeruginosa* isolates with disease tolerance[10-12,52]: in contrast with WT PAO1, the clinical strains were not lethal (Fig. 3G), provoked reduced inflammation (Fig. 3H), restricted hypothermia (Fig. S2A) and limited vascular dysfunction (Fig. S2B). The isolates exhibited ~10-fold lower pathogen burden than WT PAO1 after 24 hours, which correlated with prolonged host-pathogen coexistence (Fig. 3I, Fig 3G).

We hypothesized that the tolerogenic response to infection by the *P. aeruginosa* isolates was enabled by preservation of ATP synthase function. Compared to mice that were infected with the clinical strains and treated with a sublethal dose of the ATP synthase inhibitor oligomycin (~0.2mg/Kg) (Fig. 3J), hosts infected with the same inoculum but treated with a higher dose of oligomycin (~1.0mg/Kg) rapidly developed disease, including hypothermia (Fig. S2C) and death (Fig. 3K), indicating that it is critical for the host to conserve functional OXPHOS during infection with these clinical pathogens. The indolent infection produced by the *P. aeruginosa* isolates more closely resembled the disease caused by *ΔlptD* PAO1 (Fig. 3K). Indeed, and as observed with this mutant (Fig. 1D), the clinical strains were not as proficient at growth than WT PAO1 (Fig. 3L), suggesting that tolerance to these organisms might be linked to reduced pathogen burden. When we increased the pathogen biomass in our *in vivo* model by administering a 10-fold higher inoculum of the *P. aeruginosa* isolates (~10^7 CFUs), we observed more disease, illustrated by hypothermia and death (Fig. S2D, Fig. 3K). Thus, the tolerogenic response to the *P. aeruginosa* isolates is supported by maintenance of host ATP synthase.

P. aeruginosa isolates facilitate generation of energy in airway cells via catabolism of dietary fats –

We postulated that to stimulate pulmonary ATP synthase and thus mitigate airway inflammation, the *P. aeruginosa* isolates would enable host catabolism of fats. Fats are typically assimilated from the diet and are used to fuel OXPHOS[16,17]. During infection by the clinical pathogens, host catabolism of dietary fats would prevent the mobilization of glucose into the lung, restricting the synthesis of cytokines that rely on glycolysis. The opposite would occur during WT PAO1 infection, which depletes pulmonary ATP synthase; dietary fats would be unable to fuel energy production in pulmonary mitochondria, prompting compensatory glycolysis and cytokine release.

To stimulate OXPHOS via diet, we fed mice *ad libitum* for 1 week with a fatty acid-rich, carbohydrate-low diet (fatty acid: ~89%; carbohydrates: ~0.1%; protein: ~10%). As control, we used a fatty acid-low, carbohydrate-rich intake (fatty acid: ~10%; carbohydrates: ~80%; protein: ~10%), which induced similar animal weight than the fatty acid-rich diet (Fig. S3A). We then exposed these mice to either WT PAO1 or the *P. aeruginosa* isolates. As predicted, the levels of airway glucose in fatty-acid-fed hosts varied with the ability of the pathogen to preserve host ATP synthase: during WT PAO1 infection, BAL carbohydrate levels were significantly increased, while the opposite was observed during infection with the *P. aeruginosa* isolates (Fig. 4A). The differences in airway glucose abundance were not due to variations in pathogen burden (Fig. 4B-C) or glycemia (Fig. 4D), confirming that airway glucose concentrations depend on the ability of *P. aeruginosa* to preserve host OXPHOS.

Increased airway glucose levels in mice fed with fats and exposed to WT PAO1 correlated with the accumulation of numerous pro-inflammatory cytokines fueled by glycolysis[17,23,25,53,54], including IL-17, MCP-1, MIP-2, IL-1β, IL-1α, TNFα, MIP-1α, MIP-1β, LIX, RANTES and MIG (Fig. 4E). Conversely, during infection with the *P. aeruginosa* isolates, the reduced airway glucose levels during host fat intake limited the production of key cytokines like TNFα, MIP-1β, IL-6, IL-12p70, and G-CSF (Fig. 4F).

Using the *ΔlptD* PAO1 strain, we confirmed that glucose abundance and cytokine release in the airway of fat-fed mice were modulated by the maintenance of pulmonary ATP synthase. Compared to animals fed with the control diet, animals on the fatty-acid-rich intake and exposed to *ΔlptD* PAO1 exhibited reduced airway glucose (Fig. 4A, Fig. 4D) and cytokines, including IL-17, MCP-1, MIP-2, IL-6 and KC [17,23,25,53,54](Fig. 4G). This nutritional approach demonstrates that conservation of host ATP synthase during *P. aeruginosa* infection is central not only for airway energy generation via catabolism of fats, but also to limit inflammatory glycolysis.

Ketogenesis induced by dietary fats limits inflammatory disease during *P. aeruginosa* pneumonia –

The fatty acid-rich, carbohydrate-low diet that we used is a “ketogenic diet” that drives the generation of ketone bodies, like β-hydroxybutyrate (BHB) [29,55]. In addition to stimulating OXPHOS in peripheral tissues, ketones also suppress pathways linked to inflammatory disease, like myeloid cell recruitment[56,57] and hypothermia[28]. We observed that the ketogenic diet significantly increased systemic BHB levels during infection with both the *P. aeruginosa* isolates and WT PAO1 (Fig. 4H). During infection with the *P. aeruginosa* isolates, this diet reduced the levels of monocytes in the BAL and neutrophils in the lungs (Fig. 4I, Fig. S3B). During WT PAO1 infection, there was a significant reduction in BAL monocytes (Fig. 4J, Fig. S3C). To confirm this decrease in immune cell recruitment, we analyzed hematoxylin-eosin (H&E) stained lung sections. The ketogenic diet mitigated myeloid cell accumulation in the perivascular zone (Fig. 4K, black arrows) and in the perialveolar area (Fig. 4K, blue arrows) during WT PAO1 infection. This reduced phagocytic burden correlated with decreased lung edema (Fig. 4K, blue arrows). Similar

findings were observed during infection with the *P. aeruginosa* isolates (Fig. 4K, black/blue arrows).

In addition to suppressing phagocytic influx into the lung, we found that the ketogenic diet preserved host body temperature during pneumonia by either pathogen at early time points (Fig. 4L-M). However, the benefits of body temperature regulation were dependent on the degree of *P. aeruginosa* adaptation to the human lung, as animals infected with WT PAO1 still exhibited high mortality (Fig. 4N-O).

Ketone bodies are mobilized to the airway in response to the inhibition of host ATP synthase –

Given the importance of ketones in fueling OXPHOS and suppressing inflammation in the lung, we assessed how the host produced these metabolites in response to *P. aeruginosa* pneumonia. Animals fed a regular chow responded to *P. aeruginosa* airway infection by significantly increasing BHB release into the blood, which is a proxy for hepatic ketogenesis[29], even more so when the pathogen expressed LptD (Fig. 5A). Hepatic BHB synthesis is typically triggered by anorexia, hypoglycemia, or liver infection[51]. However, animals infected with either WT or *ΔlptD* PAO1 exhibited similar food consumption (Fig. S4A), blood glucose levels (Fig. S4B), weight loss (Fig. S4C) and pathogen burden in the liver (Fig. S4D), indicating that LptD stimulated ketone release via alternative routes. Another mechanism by which LptD might induce hepatic BHB production is by enabling LPS to enter circulation and systemically impact ATP synthase activity[58]. After being trafficked to the bacterial surface by LptD, LPS is shed as either free molecules or as part of microvesicles[59-61], accumulating in the airway of infected subjects[62,63]. This soluble LPS translocates into the bloodstream[62,63], where it can impact many tissues, including hepatocytes[28,58]. To determine if the *P. aeruginosa* LptD-LPS axis triggered hepatic ketogenesis via blockade of host ATP synthase, we treated mice with a sublethal dose of oligomycin. As anticipated, animals exposed to the ATP synthase inhibitor increased blood levels of BHB (Fig. S4E), confirming that the increase in hepatic ketogenesis during WT PAO1 infection is in response to the bioenergetic impairment imposed by LPS.

We found that hepatic ketones accumulate in the infected airway. Unbiased pathway enrichment analysis of BAL metabolites demonstrated that ketones, including BHB and acetoacetate (AcAc), were the most significantly increased metabolites in the airway of WT PAO1-infected mice compared to *ΔlptD* PAO1-exposed animals (Fig. 5B-D). This ketone accumulation was facilitated by blockade of host ATP synthase activity, as animals treated with oligomycin also exhibited greater levels of ketones in their BAL fluid (Fig. S4F).

To determine if ketones accumulate in the lung of tolerant hosts, we quantified ketone bodies in airway fluids of people with CF[2,3]. These individuals exhibited long-term colonization by different pathogens, including *P. aeruginosa* (Fig. S4G). Compared to healthy controls (HC), sputum from patients with CF exhibited significantly higher levels of BHB (Fig. 5E), confirming that ketones bodies accumulate in the airway of tolerant individuals.

Ketone bodies abrogate LPS assembly and transportation to the bacterial surface via LptD –

The accumulation of ketones in the airway presents a metabolic pressure for the bacteria. We postulated that the adaptive changes in the LPS machinery found in *P. aeruginosa* isolates from tolerant subjects were in response to the ketones enriched in the respiratory tract. LPS is formed by two covalently bound subunits: lipid A and O-antigen[64]. While O-antigen serves as a polysaccharide shield that interacts with the most immediate environment of the pathogen, lipid A attaches the toxin to the bacterial surface by embedding it in the outer membrane[64]. To efficiently anchor LPS to the outer membrane, lipid A requires "decorations" at positions 1' and 4', including arabinose molecules via *arnT* or phosphate groups via the kinase *lpxT*[64,65]. We used genome sequencing analysis of the *P. aeruginosa* isolates to examine how adaptation to the ketone-rich lung affected clusters involved in lipid A generation and decoration. Identification of non-synonymous mutations (NSM) indicated that both *arnT* and *lpxT* were the most affected loci, harboring 3 and 2 NSM, respectively (Fig. 5F). These NSMs correlated with decreased *arnT* and *lpxT* mRNA expression in the *P. aeruginosa* isolates (Fig. 5I). To synthesize O-antigen and covalently attach it to lipid A, *P. aeruginosa* employs many glycosyltransferases and ligases[64]. In the *P. aeruginosa* isolates, we observed that the most mutated genes in these routes were *WbpZ* and *WbpX,* which polymerize O-antigen, as well as *WaaL,* which binds it to lipid A, with 7, 2, and 3 NSMs, respectively (Fig. 5G-H). Most of these genetically inactivated clusters were also transcriptionally suppressed in the *P. aeruginosa* isolates (Fig. 5I).

We established that exposure of WT PAO1 to ketone bodies induces alterations in the LPS assembly pathway that are consistent with the adaptive changes found in *P. aeruginosa* isolates from tolerant subjects. Addition of AcAc, BHB, or both to glucose-rich minimal media, which facilitates LPS production[64], significantly restricted the ability of WT PAO1 to express the *arnT* locus involved in lipid A decoration (Fig. 5J). These ketones also suppressed translation of the lipid A kinase *lpxT* (Fig. 5J). This impaired *lpxT* function was corroborated by MALDI-TOF, which demonstrated smaller mass-to-charge ratio peaks at m/z= 1526, m/z= 1542, and m/z= 1696 (Fig. 5K, red arrows), a hallmark of reduced *lpxT* activity[65]. Similarly, WT PAO1 exposure to ketones restricted O-antigen synthesis (Fig. 5L) and prevented its attachment to lipid A. *WaaL,* the ligase that covalently binds these LPS components[64], was significantly depleted in the presence of AcAc, BHB, or both (Fig. 5J). Ketogenic pressure also suppressed *WpbX* and *WbpZ,* the glycosyltransferases involved in O-antigen polymerization (Fig. 5J). This impaired LPS assembly corresponded with decreased expression of *lptD* (Fig. 5J).

P. aeruginosa isolates from tolerant subjects exploit host immunometabolites to enrich ketone bodies in the lung –

Many metabolites that could impose selective pressure on *P. aeruginosa* accumulate in the airway along the course of infection. Itaconate, produced by immunoresponsive gene 1 (*Irg1*), is a major host immunoregulatory carboxylate that drives FAO[66] and tolerance to LPS-driven inflammation[67-70]. During infection with the *P. aeruginosa* isolates, but not WT PAO1, ketone bodies clustered with itaconate as the most upregulated metabolites in the

BAL fluid (Fig. S5A-B), suggesting that these isolates might exploit this immunometabolite to promote ketone concentration and patho-adaptation.

Using animals that are unable to produce itaconate (*Irg1*$^{-/-}$) and controls (*Irg1*$^{+/+}$) (Fig. 6A), we found that accumulation of BHB in the airway is *Irg1*-dependent during infection with the *P. aeruginosa* isolates, but not WT PAO1 (Fig. 6B). This *Irg1*-associated BHB accumulation was not driven by increased systemic ketones, as both *Irg1*$^{+/+}$ and *Irg1*$^{-/-}$ mice showed comparable BHB blood levels (Fig. S5C). Indeed, in contrast to hosts exposed to WT PAO1, infection with the *P. aeruginosa* isolates was associated with less BHB in circulation (Fig. S5D), which was not related to differences in food consumption, hypoglycemia, weight loss, and liver infection (Fig. S5E-H). These findings confirmed that strains from the lungs of tolerant subjects respond to *Irg1* by concentrating ketones in the respiratory tract.

Itaconate promotes altered expression of ketogenic genes in lung fibroblasts –

To identify local adjustments consistent with ketone metabolism during infection with the *P. aeruginosa* isolates, we analyzed ketogenic gene expression in each lung cell population. Ketogenesis is regulated by *Hmgcs2,* which is the rate limiting step of this pathway and is used to identify ketogenic cells[29,71]. Working in concert with other ketogenic genes like *Cpt1a, Ppara, Acat1, Hmgcl* and *Bdh1, Hmgcs2* drives the synthesis of AcAc and BHB[29]. In our scRNA-Seq analysis (Fig. S6A), we noted that fibroblasts, basophils, type 2 pneumocytes, mesothelial cells and smooth muscle cells expressed *Hmgcs2* (Fig. 6C), suggesting ketogenic metabolism in these subsets. We analyzed scRNA-seq data from *Irg1*$^{+/+}$ or *Irg1*$^{-/-}$ mice exposed to either PBS or the *P. aeruginosa* isolates, calculating a ketogenesis score for each cell subset. We then computed a Δketogenesis score ("*Irg1*$^{+/+}$" – "*Irg1*$^{-/-}$"). Volcano plots of these scores showed that *Irg1* signaling significantly enriched expression of ketogenic genes in fibroblasts during infection with the *P. aeruginosa* isolates (Fig. 6D-E). This increased ketogenic score was driven by augmented expression of *Acat1, Hmgcs2,* and *Hmgcl,* which generate AcAc, as well as *Bdh1,* which converts AcAc into BHB (Fig. 6F)[29]. During WT PAO1 infection, however, fibroblasts exhibited lower expression of many of the ketogenic genes, including *Hmgcs2, Cpt1a,* and *Bdh1,* independently of *Irg1* (Fig. 6E-F). Thus, only *P. aeruginosa* isolates that evolved in the lung of tolerant subjects co-opted itaconate to drive expression of ketogenic genes in fibroblasts.

Ketogenesis is promoted by fibroblast growth factor 21 (FGF21)[72,73]. *Irg1* enabled airway FGF21 accumulation during infection with the *P. aeruginosa* isolates (Fig. 6G), but not WT PAO1 (Fig. S6B), corroborating the link between itaconate and fibroblast pathways associated with ketogenesis in a tolerogenic environment.

Irg1 enables disease tolerance during *P. aeruginosa* lung infection –

Given its role promoting *P. aeruginosa* adaptation to the airway through ketogenesis, we postulated that itaconate facilitates host tolerance to *P. aeruginosa* disease. Compared to *Irg1*$^{-/-}$ mice, *Irg1*$^{+/+}$ animals had an increased pathogen burden during infection with the *P. aeruginosa* isolates (Fig. 6H-I). Despite this increased bacterial load, *Irg1*$^{+/+}$ mice did not exhibit worse inflammatory pathology, evidenced by identical animal survival (Fig. 6J),

similar IL-1β, IL-6, and TNFα levels (Fig. 6K), comparable albumin infiltration into the airway (Fig. S6C) and equivalent body temperature regulation (Fig. S6D). *Irg1* signaling improved host weight recovery over the course of infection with the *P. aeruginosa* isolates (Fig. 6L). We studied the impact of *Irg1* on WT PAO1 infection. While itaconate did not affect pathogen burden, IL-6, TNFα, or albumin infiltration (Fig. S6E-H), it suppressed IL-1β release (Fig. S6I). However, this attenuated inflammatory signaling was not sufficient to prevent immunopathology, as both $Irg1^{+/+}$ and $Irg1^{-/-}$ mice rapidly succumbed to WT PAO1 infection (Fig. S6J).

DISCUSSION

Our findings strongly suggest that disease tolerance in the human lung is a bilateral process based in host-pathogen metabolic remodeling. During infection with environmental *P. aeruginosa* strains that display LPS on their surface, airway cells fail to produce ATP via OXPHOS, triggering severe inflammation and alveolar destruction. This detrimental environment aggravates pathogen burden, worsening the bioenergetic interference and accelerating host demise. In response to the interruption of OXPHOS provoked by *P. aeruginosa* LPS, hepatic cells release ketone bodies into circulation, which enter the highly permeable airway compartment. These ketones restrict *P. aeruginosa* LPS assembly, selecting for less metabolically active strains compatible with airway cell OXPHOS function. Such keto-adapted *P. aeruginosa* strains limit the production of inflammatory mediators, safeguarding the alveolar tone and extending host survival. In this favorable milieu, *P. aeruginosa* exploits local immunometabolites to maintain ketone abundance, reinforcing bacterial adaptation, host-pathogen coexistence, and disease tolerance.

Maintenance of OXPHOS is an essential component of pulmonary integrity. In healthy hosts, this platform is fueled by FAO, which we show is fundamental during *P. aeruginosa* pneumonia to restrict both glycolysis and damaging inflammation[11,12,52]. In tolerant subjects, this bioenergetic circuit is preserved by ketogenesis, which typically functions to rescue the ATP homeostasis of peripheral organs. Ketogenesis selects for *P. aeruginosa* strains incapable of assembling the toxins that impair OXPHOS, preventing from the metabolo-inflammatory pathways that compromise the infected tissue: glycolysis. Ketogenesis is thus central in the conservation of the lung bioenergetic configuration that permits tolerance to *P. aeruginosa* infection[10-12].

Our findings indicate that not only the host actively responds to the pulmonary bioenergetic stress initiated by acute infection, but also the pathogen. In response to the airway ketogenic reconfiguration provoked during pneumonia, *P. aeruginosa* alters its own surface architecture, generating slow-growing strains that preserve mitochondrial bioenergetics. Other phenotypic adaptations sustain chronic *P. aeruginosa* persistence, including pro-biofilm polysaccharides, quorum sensing regulators, and drug efflux pumps[2,3,31]. These changes may reflect exposure to ketones and other tolerogenic metabolites in the airway. As we show, the diet also impacts the composition of the airway metabolome, indicating that nutrition might regulate the evolution and persistence of diverse pathogens in the human lung.

Our work provides another layer of complexity to our understanding of how ketone bodies safeguard mucosal OXPHOS during infectious diseases. This tolerogenic mechanism likely works in concert with previously established roles for ketogenesis, including inhibition of the inflammasome during intoxication with soluble LPS[58,74], and stimulation of anti-oxidant receptors like *Hcar2* (*Gpr109a*)[75]. Importantly, the impact of ketones on immunopathology varies by pathogen. In COVID-19, for example, ketone bodies support the generation of competent lymphocytes that contain the infection and promote mucosal repair[76]. Additional studies are needed to better understand how ketones influence progression of different inflammatory disease states.

By switching from systemic ketogenesis to concentration of ketones in the airway, the host response to the *P. aeruginosa* isolates limited the detrimental consequences of prolonged ketonemia[77-79]. The local augmentation of ketones promoted by the *P. aeruginosa* isolates correlated with expression of ketogenic genes in lung fibroblasts. These findings are consistent with the ketogenic role of these cells in other long-term inflammatory settings, such as cancer, where tumor-associated fibroblasts release ketone bodies as consequence of catabolic metabolism[80,81]. In the airway, fibroblasts modulate tissue repair and fibrosis, processes regulated by itaconate[82]. These findings suggest that lung fibroblasts, along with itaconate, could be targeted for the development of novel therapies to mitigate pulmonary injury during infectious diseases.

We established a link between ketogenesis, pulmonary OXPHOS maintenance, and tolerance to *P. aeruginosa* lung infection. Our findings suggest that novel therapeutic strategies for inflammatory airway diseases should consider how respiratory cells produce ATP during infection, and how this bioenergetic configuration could be targeted by either the diet or other approaches that influence the balance between OXPHOS and glycolysis.

Limitations of Study -

We appreciate that the animal models of pneumonia used in this work might not necessarily reflect the complex immunometabolic matrix of the human lung. The concentration of many metabolites found in murine fluids, such as in blood and airway, might not necessarily represent the abundance of these determinants in human tissues. Similarly, the enrichment of ketones in sputum of either healthy individuals or people with CF might be also result of different degrees of mucus accumulation, myeloid cell infiltration, dehydration, and pathogen burden. The LPS adaptation induced by ketones on *P. aeruginosa* isolates is indicative of many collaborative processes occurring in the human respiratory tract, suggesting that future studies should examine these parallel routes for a better comprehension of disease tolerance. Likewise, our assays are also limited by examining *in vitro,* but not *in vivo,* how ketones impact *P. aeruginosa* LPS assembly and transport to the surface. Although our work considered the interaction between ketogenesis and other metabolic networks, like itaconate, fatty acid oxidation, and nutrition, we did not study how these pathways associated with additional immunoregulatory platforms involved in disease tolerance. The identification of alterations in ketogenic gene expression in pulmonary fibroblasts of mice exposed to tolerogenic *P. aeruginosa* strains does not discard that many other respiratory subsets might also display similar changes in the human lung. A

more comprehensive study evaluating the crosstalk between tolerance, ketogenesis, and *P. aeruginosa* infection would support the conclusions of this manuscript.

STAR Methods

RESOURCE AVAILABILITY

Lead contact—Requests for materials and resources should be directed to and will be fulfilled by the lead contact, Sebastián A. Riquelme (sr3302@cumc.columbia.edu).

Materials availability—Bacterial strains used in this study are available from the lead contact without restriction.

Data and code availability

- single-cell RNA-seq data have been deposited at GEO (accession numbers GEO: GSE203352) and are publicly available as of the date of publication. Metabolomics data are available at Metabolights (accession numbers: MTBLS4922, MTBLS4923, and MTBLS4924). Genomes of isolates are available at NIH SRA (access numbers: PA270 (SRR8775051), PA338 (SRR8775050), PA339 (SRR8775058), PA599 (SRR8775057), PA600 (SRR8775065), PA601 (SRR8775054), PA602 (SRR8775055), PA603 (SRR8775053), PA604 (SRR8775056), PA605 (SRR8775052), PA606 (SRR8775060), PA607 (SRR8775059), PA608 (SRR8775062), PA683 (SRR8775061), PA684 (SRR8775064), PA685 (SRR8775063) and PA686 (SRR8775066). The accession numbers are also listed in the Key resources table.
- This paper does not report original code.
- Data S1 represents an Excel file containing the values that were used to create all the graphs in the paper, as well as gels in Figures 1A, 1E, 3C and 5L. Any additional information required to reanalyze the data reported in this paper is available from the lead contact upon request.

EXPERIMENTAL MODEL AND STUDY PARTICIPANT DETAILS

Mice experiments—All animal experiments were performed following institutional guidelines at Columbia University. Mice studies were approved by protocol IACUC AABE8600. 8–10-week-old WT C57bl/6 mice (20-25grs) were obtained from The Jackson Laboratories. *Irg1*$^{-/-}$ (*Acod1*$^{-/-}$) and *Ilr1*$^{-/-}$ mice were also obtained from The Jackson Laboratories and bred in our facilities at Columbia University Medical Center. WT, *Irg1*$^{-/-}$, and *Ilr1*$^{-/-}$ mice are immunocompetent animals, and they received neither medical nor drug treatments prior to infection. Each *in vivo* experiment was performed using 50% female and 50% male animals, and results were not expected to be influenced by sex. Animals were randomly assigned to cages, and maintained under regular rodent light/dark cycles, 18-23°C. Unless otherwise indicated, mice were fed with a regular irradiated chow, Purina 5053 (~25% protein, ~62% carbohydrate, ~13% fat).

Human samples—Ketones in human samples were measured in sputum from 5 healthy controls (HC) and 9 subjects with CF, all adults. Male and female samples were collected in an approximate 50%–50% ratio. These samples were kindly provided by Dr. Clemente Britto-Leon from Yale University. An informed consent was signed by all subjects providing samples. These studies were performed under our approved IRB protocol AAAR1395.

***P. aeruginosa* strains—**WT PAO1 and *ΔlptD* PAO1 were grown in LB overnight and sub-cultured until exponential phase for studies. *P. aeruginosa* strains from CF#1 were from a 10-year chronically infected CF patient. *P. aeruginosa* strains from CF#2 were recovered from a 12-year chronically infected CF individual. All *P. aeruginosa* isolates from CF#1 and CF#2 were part of longitudinal collections. *P. aeruginosa* isolates from 10 ICU patients were obtained at Columbia University Irving Medical Center facilities. These subjects were acutely infected for at least 3-5 days. These studies were performed under our approved IRB protocols AAAR1395 and AAAS6553. All these strains were plated in LB agar and their phenotypes were characterized regarding small colony variants or mucoid morphology. Infection experiments with these clinical isolates were performed from LB subcultures on exponential phase of growth, which derived from overnight grown stocks. Overnight cultures and subcultures were grown at 37°C under shacking.

METHOD DETAILS

Oxygen consumption rate measurements in macrophages—Mouse bone-marrow derived macrophages (BMDMs) were exposed at 37°C for 3h to either PBS, 50ug/ml LPS, WT PAO1, or *ΔlptD* PAO1 at multiplicity of infection (MOI) = 10. Then, via Seahorse technology, oxygen consumption rate (OCR) was tracked in these cells using commercially obtained plates as recommended by the manufacturer.

***P. aeruginosa* consumption of NADH and FADH2—**Both WT PAO1 and *ΔlptD* PAO1 were grown until exponential phase and applied at same concentration to a Biolog 96-well plate array where each well contained a single carbon source (Mitoplate S1). For these assays, we followed the instructions provided by the manufactures. Plates were incubated at 37°C for 48h-72 h and then absorbances were measured at OD_{400nm}.

Infection of mice with *P. aeruginosa* strains—Animals used were WT, *Irg1*$^{-/-}$ (*Acod1*$^{-/-}$), or *Il1r*$^{-/-}$ C57bl/6 mice. Animals were exposed to either PBS, WT PAO1, *ΔlptD* PAO1 or the *P. aeruginosa* isolates. When indicated, the bacterial dose varied accordingly with the experiment performed. We used different inoculum: ~10^5, ~10^6 or ~10^7 CFUs or PBS alone (non-infected); in the mix of the *P. aeruginosa* isolates, equal parts of each individual strain were used to form the desired inoculum. When indicated, animals were administered or not during the infection either 0.2mg/Kg or 1.0mg/Kg of oligomycin. Similarly, when indicated, 24h prior and during the moment of the infection, animals were treated or not with 20mg/Kg of etomoxir. Survival of mice was monitored for 5 days. When indicated, animal temperature was tracked with an infrared thermometer that measured surface and internal temperature. To evaluate the host immune response to infection, mice were sacrificed 24h after exposure to the pathogens, and BAL and lungs were collected. CFU amounts were quantified by LB

agar plating. CFUs below limit of detection (10^2 CFU per tissue) were represented in graphs as "non-detected" (ND). Immune cells (flow cytometry) and cytokines (ELISA) were quantified in BAL and in lungs. Flow cytometry: alveolar macrophages were $CD45^+CD11b^{low/-}SiglecF^{high}CD11c^+CD193^-Ly6G^-Ly6C^-$, neutrophils were $CD45^+CD11b^{high}SiglecF^{low/-}CD11c^-MHCII^-CD193^-Ly6G^+Ly6C^{low/-}$, and monocytes were $CD45+CD11b^{high}SiglecF^{low/-}CD11c^-MHCII^-CD193^-Ly6G^-Ly6C^{low/high}$. Samples were analyzed with FlowJo, vX. Cell viability was determined by using live/dead DAPI staining (Thermo Fisher Scientific, L34962). These animals were controlled for ketosis via quantification of β-hydroxybutyrate (BHB) at the beginning of the light cycle (between 8:00am-9:00am) using KetoBM Ketone Strips and the KetoBM Blood Ketone Meter Kit for Keto Diet Testing. We also measured glycemia by using the AUVON I-QARE DS-W Draw-in Blood Glucose Test Strips system together with the AUVON DS-W Diabetes Sugar Testing Meter. When indicated, BAL were analyzed by Mass-Spec for metabolomics studies.

Food consumption during infection of mice with *P. aeruginosa* strains—To track mouse food consumption and weight, mice were individually placed in separated cages (1 animal/cage). After exposure of these animals to PBS or infected either with WT PAO1, *ΔlptD* PAO1, or the *P. aeruginosa* isolates (from CF#2), we monitored food consumption by weighting the amount of food before and after infection, every 24h. We performed an exhaustive examination of each cage to confirm that the food counted as consumed was not found in the cage. Similarly, we tracked daily animal weight using a digital scale.

Airway metabolomics—BAL from either non-infected or 24h-infected mice were collected with 3ml of sterile PBS. Samples were immediately placed on ice. Then, samples were diluted with 100% methanol in a 1:1 proportion, mixed and stored at −80°C for future metabolomics analysis. Just prior to mass spectrometry, samples were thawed and dried under a stream of N_2 and were resuspended in HPLC-grade water at a 4:1 dilution (relative to the original BAL volume). High-resolution mass spectrometry data were acquired on a Thermo Fisher Exactive Mass spectrometer in negative mode using 25 min reverse phase gradients and ion-pairing chromatography. Metabolites were identified using the known chromatographic retention times of standards, and metabolite signals were quantified using MAVEN. Metabolite signal intensities were used to quantify difference between treatments in BAL and respect to PBS-treated animals.

Lung tissue histopathology studies—Mice aged 8–10 weeks were intranasally exposed to either PBS, WT PAO1, or the *P. aeruginosa* isolates.Then, 24h later, animals were sacrificed and a canula was inserted into the trachea and tied with suture. The thorax was opened, and the lungs were fixed by gentle infusion of formalin-free tissue fixative through the canula from a syringe positioned 5cm above the mouse. The whole lungs were excised and placed in formalin-free tissue fixative for 24h before transfer to 70% ethanol. The tissue was paraffinized, and two 5mm sections were taken 25mm apart. The slices were then stained with hematoxylin and eosin and scored by a pathologist, who was blinded to the sample identities. Immune cell infiltration and edema were examined by light microscopy.

Diets for *in vivo* assays—When indicated, animals were fed a ketogenic diet (D10070801i, Research Diets, Inc) or a carbohydrate-rich control diet (D19082304i, Research diets, Inc) for 1 week (*ad libitum*). Ketogenic diet contained ~10% protein, ~0.1% carbohydrate, ~88.9% fat (%Kcal). Control diet contained ~10% protein, ~80% carbohydrate, ~10% fat (%Kcal). After one week, mice were intranasally infected with ~10^6 CFU of the *P. aeruginosa* isolates, WT PAO1, or *ΔlptD* PAO1. 24h later, animals were processed. When indicated, blood was obtained from the tail of these animals and glycemia and ketosis were measured by using draw-in blood test strips for glucose and β-hydroxybutyrate, respectively.

Mouse lung processing for single-cell RNA-Sequencing analysis—WT or *Irg1*$^{-/-}$ C57bl/6 mice (8-10 week old) were treated with PBS or infected either with WT PAO1 or the *P. aeruginosa* clinical isolates (~10^6 total CFU per mouse in 50uL). 24h after infection, mice were euthanized, their lungs were harvested, and single cell suspensions of the lungs were prepared as described. Briefly, the lungs were placed in an Eppendorf tube containing an enzymatic digestion solution of collagenase I (2 mg/mL), dispase (20 mg/mL), elastase (1 mg/mL), and DNAse (1 uL/mL) in PBS. The lungs were minced within the tube and then incubated with shaking at 37°C for 30 minutes. 4 volumes of PBS supplemented with 10% FBS was added to quench the digestion, and the digestion solution was strained over a 70-micron filter. The cell suspension was spun down at 4°C and 1400 rpm for 7 min. Red blood cell lysis was performed using the Invitrogen RBC lysis buffer. The resulting cell pellet was resuspended in PBS supplemented with 0.04% BSA before being loaded onto the 10X Genomics Chromium Single Cell Controller. Cell viability analysis was performed before loading the samples, and was above 95% per sample. A total of ~8000 cells were analyzed per sample. FASTQ file generation, alignment, filtering, barcode counting, and UMI counting were done using the 10X Cell Ranger software.

Single cell RNA-Sequencing analysis—Matrix data generated by scRNA-Seq were analyzed using the Seurat library (https://satijalab.org) in R Studio (https://www.rstudio.com). Data were cleaned for mitochondrial RNA (less than 5% per sample), and unbiased cell clustering was performed. The Seurat algorithm identified 23 cell clusters with unique transcriptomic signatures. To determine the biological nature of each one of these clusters, we did comparative analyses of the transcriptomic profile of each cluster with available data bases using the SingleR algorithm (using ImmGen as the reference data set). In addition, this cluster characterization was manually cross-checked with cell markers from publicly available datasets using the top 10 markers for each cluster. Scores for ketogenic routes were calculated using the AddModuleScore function in Seurat. Briefly, ketogenic scores included the following genes: *Hmgcs2, Bdh1, Hmgcl, Acat1, Ppara* and *Cpt1a.* We calculated ketogenic scores for each either WT or *Irg1*$^{-/-}$ pulmonary subset, exposed or not to WT PAO1 or the *P. aeruginosa* isolates. Then, via a MAST statistical test, we determined differences between treatments in the same pulmonary subset, and computed a "−Log(*P*-value)". To establish if *Irg1* promoted enrichment of decrease of this ketogenic score in a specific pulmonary subset, we subtracted the ketogenic score obtained in the *Irg1*$^{-/-}$ background from WT controls (Δketogenesis score ("*Irg1*$^{+/+}$" – "*Irg1*$^{-/-}$")). Then,

for each pulmonary cell type, we performed volcano plots illustrating in the Y axis the "−Log(*P*-value)" and in the X coordinate the Δketogenesis score.

qRT-PCR for genes in *P. aeruginosa* exposed to ketones—WT PAO1 was grown in LB overnight and then subcultured until exponential phase in M9 supplemented with glucose, glucose + BHB, glucose + AcAc, or glucose + BHB + AcAc (7mM each metabolite). Total RNA was extracted using either the E.Z.N.A. Total RNA Kit1 or RNeasy Mini Kit. The RNA was then processed with DNase. The RNA concentration was measured using NanoDrop One. cDNA was synthesized using High-Capacity cDNA Reverse Transcription Kit (Applied Biosystems), and qPCR was performed with a StepOnePlus Real-Time PCR System (Applied Biosystems) using POWER SYBR Green PCR Master Mix (Applied Biosystems). Sequences of the primers used for qRT-PCRs are listed in Key Resource Table. Relative gene expression was calculated by the $2^{-\Delta\Delta CT}$ method. The *rpsL* transcript was used as a reference housekeeping gene, and the WT PAO1 strain grown in glucose was used as a calibrator. When studying clinical isolates, these strains were grown in LB overnight and then subcultured in the same conditions until exponential phase. Then, total RNA extracted and qRT-PCR were performed.

LPS assembly studies in WT PAO1—To visualize the O-antigen and lipid A in WT PAO1 exposed to ketones, LPS was first isolated using a hot phenol extraction from overnight cultures normalized to OD_{600}=0.5 after 1:10 dilution. Samples were treated with DNase and RNase for 30min at 37°C and Proteinase K at 59C overnight. After hot phenol extraction with Trizol, the isolated LPS was run on a Tricine 10%–20% gel. The gel was then stained using Pro-Q Emerald 300 Lipopolysaccharide Gel Stain Kit and imaged using UV light on a Protein Simple imager.

Pathway analysis of airway fluids—Curated metabolomics data from airway fluids of both control and bacteria-exposed mice were submitted to MetaboloAnalyst 5.0 (https://www.metaboanalyst.ca). Data were analyzed through Enrichment Analysis, using the Kyoto Encyclopedia of Genes and Genomes (KEGG) database as reference. To maintain unbiased interpretation of the data, we utilized the graphs provided by the platform.

P. aeruginosa* lipid A isolation and analysis—P. aeruginosa* WT PAO1 was cultured overnight in LB, then washed, and subcultured in M9 media containing either glucose (7mM) alone or glucose (7mM), BHB (7mM), and AcAc (7mM). Bacteria were grown until exponential phase at 37°C with shaking. Lipid A was extracted from cell pellets using an ammonium hydroxide-isobutyric acid-based procedure. Approximately 5 mL of cell culture was pelleted and resuspended in 400 μl of 70% isobutyric acid (Sigma, I1754) and 1 M ammonium hydroxide (Sigma, 221228), (5:3 v/v). Samples were incubated for 1 h at 100°C and centrifuged at 8,000 × g for 5 min. Supernatants were collected, added to endotoxin-free water (1:1 v/v), snap-frozen on dry ice, and lyophilized overnight. The resultant material was washed twice with 1 mL methanol (Thermo Fisher Scientific, A456-1), and lipid A was extracted using 80 μl of a mixture of chloroform (Thermo Fisher Scientific, C606SK-4), methanol, and water (3:1:0.25 v/v/v). Once extracted, 1 μl of the concentrate was spotted on a steel re-usable MALDI plate (Hudson Surface Technology, PL-PD-000040-P) followed

by 1 μl of 10 mg/mL norharmane matrix (Sigma, NG252) in chloroform-methanol (2:1 v/v, Sigma) and air-dried. All samples were analyzed on a Bruker Microflex mass spectrometer (Bruker Daltonics) in the negative-ion mode with reflectron mode. An electrospray tuning mix (Agilent, G2421A) was used for mass calibration. Spectral data were analyzed with Bruker Daltonics FlexAnalysis software (v4.30). The resulting spectra were used to estimate the lipid A structures present in each condition based on their predicted structures and molecular weights.

Lung protein extraction and western blots—Total lung tissue was removed from WT mice exposed for 24h to either PBS, WT PAO1, *ΔlptD* PAO1 or the *P. aeruginosa* isolates. Single cell fractions were prepared, washed, and resuspended for 30min in 300uL of RIPA buffer containing protease/phosphatase inhibitors at 4°C. Samples were centrifuged for 25min at 15,000g and the supernatant was recovered and stored at −80°C. To perform western blots, samples were denatured at 37°C for 20min and ran in 4-12% gels in MES buffer. To stain actin, we used a monoclonal anti-β-actin antibody produced in mouse (Sigma, Cat A5441). To mark OXPHOS components, we used an OXPHOS rodent WB antibody cocktail (Thermo Fisher Scientific, 45-8099). To detect hexokinase-2, we used a hexokinase 2 polyclonal antibody (Thermo Fisher Scientific, 22029-1-AP). Membranes were transferred using iblot and stained overnight with primary antibodies. Then, samples were washed and incubated for 1h with the HRP-tagged secondary antibody. Membranes were revealed and analyzed for protein expression.

Whole genome sequencing and single-nucleotide polymorphism (SNP) calling in *P. aeruginosa* isolates—*P. aeruginosa* isolates were grown overnight in LB broth at 37°C. Genomic DNA was extracted using the Wizard Genomic DNA Purification Kit (Promega) according to manufacturer instructions. Genomic DNA libraries were prepped using the Nextera XT kit and sequenced on a HiSeq 2500 sequencer (Illumina) with 125-bp paired-end reads. Genome assembly was done using the paired-end implementation of ABySS. For single-nucleotide polymorphism (SNP) calling, were compared SNPs between isolates and WT PAO1. This was done by means of short-read alignment to the genome of PAO1 as reference (GenBank: AE004091), using the Burrows–Wheeler alignment (bwa) tool (available at: http://bio-bwa.sourceforge.net). SNP calls were made using samtools (available at: http://samtools.sourceforge.net). SNPs that were not listed as heterozygous and had a per base Q score ≥20 were defined as high quality. Samples can be found at NIH SRA with the following codes: PA270 (SRR8775051), PA338 (SRR8775050), PA339 (SRR8775058), PA599 (SRR8775057), PA600 (SRR8775065), PA601 (SRR8775054), PA602 (SRR8775055), PA603 (SRR8775053), PA604 (SRR8775056), PA605 (SRR8775052), PA606 (SRR8775060), PA607 (SRR8775059), PA608 (SRR8775062), PA683 (SRR8775061), PA684 (SRR8775064), PA685 (SRR8775063) and PA686 (SRR8775066).

QUANTIFICATION AND STATISTICAL ANALYSIS

We modeled the number of independent experiments required to reach significance between groups by using JMP, a computer program dedicated for statistical analysis. We based this simulation on preliminary data, experimental design, and past experience. These analyses

were done assuming a 20% standard deviation (SD), and equivalent variances within groups. Significance ($P < 0.05$) with power 0.8 was used. Experiments in this study were not performed in a blinded fashion. All analyses and graphs were performed using the GraphPad Prism 9 software. Data in graphs are shown as average ± SEM and data were assumed to fit normal distribution. For comparison between average values for more than 2 groups, we performed One-Way ANOVA with a multiple posteriori comparison. When studying two or more group along time, data was analyzed using Two-Way ANOVA with a multiple posteriori comparison. Differences between two groups in samples' average values were analyzed using analysis of variance (parametric) or Student's t test for normally distributed data or Mann-Whitney or Kruskal-Wallis test otherwise. Differences were considered significant when P value (two-sides) was under 0.05 ($P < 0.05$). Significances P values and amounts of independent experiments and replicates are indicated in each Figure Legend.

Supplementary Material

Refer to Web version on PubMed Central for supplementary material.

Acknowledgements

This study was funded by grants R35GM146776 (NIH), RIQUEL21I0 (CFF), and GT007268 (Innovation Nucleation Fund) awarded to S.A.R. K.L.T. was supported by NIH grant 1F30AI161801, T.W.F.L. was supported by NIH grant K99HL157550, and A.S.P. was supported by NIH grant 1R35HL135800 and CFF grant 003028G221. We thank the Single Cell Core at the Columbia University Genome Center and the Molecular Pathology Core at Columbia University for their technical help with scRNA-sequencing and histology studies. We thank Dr. Ian Lewis and Marija Drikic at University of Calgary, Alberta, Canada, for their help with metabolomic studies. We thank Dr. Paul Planet and Dr. Ahmed Moustafa at Children's Hospital of Philadelphia, USA, for their help on bacterial genome sequencing analyses. We thank Dr. Clemente Britto-Leon at Yale University, USA, for providing sputum samples. This publication is also supported by the CCTI Flow Cytometry Core at CUIMC (NIH S10RR027050).

Inclusion and diversity

We support inclusive, diverse, and equitable conduct of research.

References

1. Lin CK, and Kazmierczak BI (2017). Inflammation: A Double-Edged Sword in the Response to Pseudomonas aeruginosa Infection. J Innate Immun 9, 250–261. 10.1159/000455857. [PubMed: 28222444]
2. Faure E, Kwong K, and Nguyen D (2018). Pseudomonas aeruginosa in Chronic Lung Infections: How to Adapt Within the Host? Front Immunol 9, 2416. 10.3389/fimmu.2018.02416. [PubMed: 30405616]
3. Winstanley C, O'Brien S, and Brockhurst MA (2016). Pseudomonas aeruginosa Evolutionary Adaptation and Diversification in Cystic Fibrosis Chronic Lung Infections. Trends Microbiol 24, 327–337. 10.1016/j.tim.2016.01.008. [PubMed: 26946977]
4. Hilliam Y, Moore MP, Lamont IL, Bilton D, Haworth CS, Foweraker J, Walshaw MJ, Williams D, Fothergill JL, De Soyza A, and Winstanley C (2017). Pseudomonas aeruginosa adaptation and diversification in the non-cystic fibrosis bronchiectasis lung. Eur Respir J 49. 10.1183/13993003.02108-2016.
5. Chalmers JD, and Hill AT (2013). Mechanisms of immune dysfunction and bacterial persistence in non-cystic fibrosis bronchiectasis. Mol Immunol 55, 27–34. 10.1016/j.molimm.2012.09.011. [PubMed: 23088941]

6. Martinez-Solano L, Macia MD, Fajardo A, Oliver A, and Martinez JL (2008). Chronic Pseudomonas aeruginosa infection in chronic obstructive pulmonary disease. Clin Infect Dis 47, 1526–1533. 10.1086/593186. [PubMed: 18990062]
7. Rodrigo-Troyano A, Melo V, Marcos PJ, Laserna E, Peiro M, Suarez-Cuartin G, Perea L, Feliu A, Plaza V, Faverio P, et al. (2018). Pseudomonas aeruginosa in Chronic Obstructive Pulmonary Disease Patients with Frequent Hospitalized Exacerbations: A Prospective Multicentre Study. Respiration 96, 417–424. 10.1159/000490190. [PubMed: 30041176]
8. Wijers CD, Chmiel JF, and Gaston BM (2017). Bacterial infections in patients with primary ciliary dyskinesia: Comparison with cystic fibrosis. Chron Respir Dis 14, 392–406. 10.1177/1479972317694621. [PubMed: 29081265]
9. Cohen-Cymberknoh M, Weigert N, Gileles-Hillel A, Breuer O, Simanovsky N, Boon M, De Boeck K, Barbato A, Snijders D, Collura M, et al. (2017). Clinical impact of Pseudomonas aeruginosa colonization in patients with Primary Ciliary Dyskinesia. Respir Med 131, 241–246. 10.1016/j.rmed.2017.08.028. [PubMed: 28947038]
10. Martins R, Carlos AR, Braza F, Thompson JA, Bastos-Amador P, Ramos S, and Soares MP (2019). Disease Tolerance as an Inherent Component of Immunity. Annu Rev Immunol 37, 405–437. 10.1146/annurev-immunol-042718-041739. [PubMed: 30673535]
11. Schneider DS, and Ayres JS (2008). Two ways to survive infection: what resistance and tolerance can teach us about treating infectious diseases. Nat Rev Immunol 8, 889–895. 10.1038/nri2432. [PubMed: 18927577]
12. Soares MP, Teixeira L, and Moita LF (2017). Disease tolerance and immunity in host protection against infection. Nat Rev Immunol 17, 83–96. 10.1038/nri.2016.136. [PubMed: 28044057]
13. Liu G, and Summer R (2019). Cellular Metabolism in Lung Health and Disease. Annu Rev Physiol 81, 403–428. 10.1146/annurev-physiol-020518-114640. [PubMed: 30485759]
14. Tsitoura E, Vasarmidi E, Bibaki E, Trachalaki A, Koutoulaki C, Papastratigakis G, Papadogiorgaki S, Chalepakis G, Tzanakis N, and Antoniou KM (2019). Accumulation of damaged mitochondria in alveolar macrophages with reduced OXPHOS related gene expression in IPF. Respir Res 20, 264. 10.1186/s12931-019-1196-6. [PubMed: 31775876]
15. Cloonan SM, Kim K, Esteves P, Trian T, and Barnes PJ (2020). Mitochondrial dysfunction in lung ageing and disease. Eur Respir Rev 29. 10.1183/16000617.0165-2020.
16. Mills EL, Kelly B, Logan A, Costa ASH, Varma M, Bryant CE, Tourlomousis P, Dabritz JHM, Gottlieb E, Latorre I, et al. (2016). Succinate Dehydrogenase Supports Metabolic Repurposing of Mitochondria to Drive Inflammatory Macrophages. Cell 167, 457–470 e413. 10.1016/j.cell.2016.08.064. [PubMed: 27667687]
17. Tannahill GM, Curtis AM, Adamik J, Palsson-McDermott EM, McGettrick AF, Goel G, Frezza C, Bernard NJ, Kelly B, Foley NH, et al. (2013). Succinate is an inflammatory signal that induces IL-1beta through HIF-1alpha. Nature 496, 238–242. 10.1038/nature11986. [PubMed: 23535595]
18. Cloonan SM, and Choi AM (2016). Mitochondria in lung disease. J Clin Invest 126, 809–820. 10.1172/JCI81113. [PubMed: 26928034]
19. Nam HS, Izumchenko E, Dasgupta S, and Hoque MO (2017). Mitochondria in chronic obstructive pulmonary disease and lung cancer: where are we now? Biomark Med 11, 475–489. 10.2217/bmm-2016-0373. [PubMed: 28598223]
20. Kandasamy J, Rezonzew G, Jilling T, Ballinger S, and Ambalavanan N (2019). Mitochondrial DNA variation modulates alveolar development in newborn mice exposed to hyperoxia. Am J Physiol Lung Cell Mol Physiol 317, L740–L747. 10.1152/ajplung.00220.2019. [PubMed: 31432715]
21. Aghapour M, Remels AHV, Pouwels SD, Bruder D, Hiemstra PS, Cloonan SM, and Heijink IH (2020). Mitochondria: at the crossroads of regulating lung epithelial cell function in chronic obstructive pulmonary disease. Am J Physiol Lung Cell Mol Physiol 318, L149–L164. 10.1152/ajplung.00329.2019. [PubMed: 31693390]
22. Mason RJ (2006). Biology of alveolar type II cells. Respirology 11 Suppl, S12–15. 10.1111/j.1440-1843.2006.00800.x. [PubMed: 16423262]
23. Everts B, Amiel E, Huang SC, Smith AM, Chang CH, Lam WY, Redmann V, Freitas TC, Blagih J, van der Windt GJ, et al. (2014). TLR-driven early glycolytic reprogramming via the kinases

TBK1-IKKvarepsilon supports the anabolic demands of dendritic cell activation. Nat Immunol 15, 323–332. 10.1038/ni.2833. [PubMed: 24562310]

24. Everts B, Amiel E, van der Windt GJ, Freitas TC, Chott R, Yarasheski KE, Pearce EL, and Pearce EJ (2012). Commitment to glycolysis sustains survival of NO-producing inflammatory dendritic cells. Blood 120, 1422–1431. 10.1182/blood-2012-03-419747. [PubMed: 22786879]
25. Ryan DG, and O'Neill LAJ (2020). Krebs Cycle Reborn in Macrophage Immunometabolism. Annu Rev Immunol 38, 289–313. 10.1146/annurev-immunol-081619-104850. [PubMed: 31986069]
26. Cohen TS, and Prince AS (2013). Activation of inflammasome signaling mediates pathology of acute P. aeruginosa pneumonia. J Clin Invest 123, 1630–1637. 10.1172/JCI66142. [PubMed: 23478406]
27. Riquelme SA, Hopkins BD, Wolfe AL, DiMango E, Kitur K, Parsons R, and Prince A (2017). Cystic Fibrosis Transmembrane Conductance Regulator Attaches Tumor Suppressor PTEN to the Membrane and Promotes Anti Pseudomonas aeruginosa Immunity. Immunity 47, 1169–1181 e1167. 10.1016/j.immuni.2017.11.010. [PubMed: 29246444]
28. Ganeshan K, Nikkanen J, Man K, Leong YA, Sogawa Y, Maschek JA, Van Ry T, Chagwedera DN, Cox JE, and Chawla A (2019). Energetic Trade-Offs and Hypometabolic States Promote Disease Tolerance. Cell 177, 399–413 e312. 10.1016/j.cell.2019.01.050. [PubMed: 30853215]
29. Puchalska P, and Crawford PA (2017). Multi-dimensional Roles of Ketone Bodies in Fuel Metabolism, Signaling, and Therapeutics. Cell Metab 25, 262–284. 10.1016/j.cmet.2016.12.022. [PubMed: 28178565]
30. Cahill GF Jr. (2006). Fuel metabolism in starvation. Annu Rev Nutr 26, 1–22. 10.1146/annurev.nutr.26.061505.111258. [PubMed: 16848698]
31. Planet PJ (2022). Adaptation and Evolution of Pathogens in the Cystic Fibrosis Lung. J Pediatric Infect Dis Soc 11, S23–S31. 10.1093/jpids/piac073. [PubMed: 36069898]
32. Riquelme SA, Liimatta K, Wong Fok Lung T, Fields B, Ahn D, Chen D, Lozano C, Saenz Y, Uhlemann AC, Kahl BC, et al. (2020). Pseudomonas aeruginosa Utilizes Host-Derived Itaconate to Redirect Its Metabolism to Promote Biofilm Formation. Cell Metab 31, 1091–1106 e1096. 10.1016/j.cmet.2020.04.017. [PubMed: 32428444]
33. Lo Sciuto A, Martorana AM, Fernandez-Pinar R, Mancone C, Polissi A, and Imperi F (2018). Pseudomonas aeruginosa LptE is crucial for LptD assembly, cell envelope integrity, antibiotic resistance and virulence. Virulence 9, 1718–1733. 10.1080/21505594.2018.1537730. [PubMed: 30354941]
34. Konovalova A, Kahne DE, and Silhavy TJ (2017). Outer Membrane Biogenesis. Annu Rev Microbiol 71, 539–556. 10.1146/annurev-micro-090816-093754. [PubMed: 28886680]
35. Huus KE, Joseph J, Zhang L, Wong A, Aaron SD, Mah TF, and Sad S (2016). Clinical Isolates of Pseudomonas aeruginosa from Chronically Infected Cystic Fibrosis Patients Fail To Activate the Inflammasome during Both Stable Infection and Pulmonary Exacerbation. J Immunol 196, 3097–3108. 10.4049/jimmunol.1501642. [PubMed: 26895832]
36. Bhagirath AY, Li Y, Somayajula D, Dadashi M, Badr S, and Duan K (2016). Cystic fibrosis lung environment and Pseudomonas aeruginosa infection. BMC Pulm Med 16, 174. 10.1186/s12890-016-0339-5. [PubMed: 27919253]
37. Muhlebach MS, Zorn BT, Esther CR, Hatch JE, Murray CP, Turkovic L, Ranganathan SC, Boucher RC, Stick SM, and Wolfgang MC (2018). Initial acquisition and succession of the cystic fibrosis lung microbiome is associated with disease progression in infants and preschool children. PLoS Pathog 14, e1006798. 10.1371/journal.ppat.1006798. [PubMed: 29346420]
38. Balibar CJ, and Grabowicz M (2016). Mutant Alleles of lptD Increase the Permeability of Pseudomonas aeruginosa and Define Determinants of Intrinsic Resistance to Antibiotics. Antimicrob Agents Chemother 60, 845–854. 10.1128/AAC.01747-15. [PubMed: 26596941]
39. Song J, Steidle L, Steymans I, Singh J, Sanner A, Bottinger L, Winter D, and Becker T (2023). The mitochondrial Hsp70 controls the assembly of the F(1)F(O)-ATP synthase. Nat Commun 14, 39. 10.1038/s41467-022-35720-5. [PubMed: 36596815]
40. Smeitink J, van den Heuvel L, and DiMauro S (2001). The genetics and pathology of oxidative phosphorylation. Nat Rev Genet 2, 342–352. 10.1038/35072063. [PubMed: 11331900]

41. Wilson DF (2017). Oxidative phosphorylation: regulation and role in cellular and tissue metabolism. J Physiol 595, 7023–7038. 10.1113/JP273839. [PubMed: 29023737]
42. Wolf AJ, Reyes CN, Liang W, Becker C, Shimada K, Wheeler ML, Cho HC, Popescu NI, Coggeshall KM, Arditi M, and Underhill DM (2016). Hexokinase Is an Innate Immune Receptor for the Detection of Bacterial Peptidoglycan. Cell 166, 624–636. 10.1016/j.cell.2016.05.076. [PubMed: 27374331]
43. Meylan S, Porter CBM, Yang JH, Belenky P, Gutierrez A, Lobritz MA, Park J, Kim SH, Moskowitz SM, and Collins JJ (2017). Carbon Sources Tune Antibiotic Susceptibility in Pseudomonas aeruginosa via Tricarboxylic Acid Cycle Control. Cell Chem Biol 24, 195–206. 10.1016/j.chembiol.2016.12.015. [PubMed: 28111098]
44. Jones N, Blagih J, Zani F, Rees A, Hill DG, Jenkins BJ, Bull CJ, Moreira D, Bantan AIM, Cronin JG, et al. (2021). Fructose reprogrammes glutamine-dependent oxidative metabolism to support LPS-induced inflammation. Nat Commun 12, 1209. 10.1038/s41467-021-21461-4. [PubMed: 33619282]
45. Vijayan V, Pradhan P, Braud L, Fuchs HR, Gueler F, Motterlini R, Foresti R, and Immenschuh S (2019). Human and murine macrophages exhibit differential metabolic responses to lipopolysaccharide - A divergent role for glycolysis. Redox Biol 22, 101147. 10.1016/j.redox.2019.101147. [PubMed: 30825774]
46. Symersky J, Osowski D, Walters DE, and Mueller DM (2012). Oligomycin frames a common drug-binding site in the ATP synthase. Proc Natl Acad Sci U S A 109, 13961–13965. 10.1073/pnas.1207912109. [PubMed: 22869738]
47. Schlaepfer IR, and Joshi M (2020). CPT1A-mediated Fat Oxidation, Mechanisms, and Therapeutic Potential. Endocrinology 161. 10.1210/endocr/bqz046.
48. Divakaruni AS, Hsieh WY, Minarrieta L, Duong TN, Kim KKO, Desousa BR, Andreyev AY, Bowman CE, Caradonna K, Dranka BP, et al. (2018). Etomoxir Inhibits Macrophage Polarization by Disrupting CoA Homeostasis. Cell Metab 28, 490–503 e497. 10.1016/j.cmet.2018.06.001. [PubMed: 30043752]
49. Kowalski ML, Didier A, and Kaliner MA (1989). Neurogenic inflammation in the airways. I. Neurogenic stimulation induces plasma protein extravasation into the rat airway lumen. Am Rev Respir Dis 140, 101–109. 10.1164/ajrccm/140.1.101. [PubMed: 2751157]
50. Minakata Y, Nakanishi M, Hirano T, Matsunaga K, Yamagata T, and Ichinose M (2005). Microvascular hyperpermeability in COPD airways. Thorax 60, 882. 10.1136/thx.2005.045765.
51. Tirosh I, Izar B, Prakadan SM, Wadsworth MH 2nd, Treacy D, Trombetta JJ, Rotem A, Rodman C, Lian C, Murphy G, et al. (2016). Dissecting the multicellular ecosystem of metastatic melanoma by single-cell RNA-seq. Science 352, 189–196. 10.1126/science.aad0501. [PubMed: 27124452]
52. McCarville JL, and Ayres JS (2018). Disease tolerance: concept and mechanisms. Curr Opin Immunol 50, 88–93. 10.1016/j.coi.2017.12.003. [PubMed: 29253642]
53. Bechara R, McGeachy MJ, and Gaffen SL (2021). The metabolism-modulating activity of IL-17 signaling in health and disease. J Exp Med 218. 10.1084/jem.20202191.
54. Shanmugam N, Reddy MA, Guha M, and Natarajan R (2003). High glucose-induced expression of proinflammatory cytokine and chemokine genes in monocytic cells. Diabetes 52, 1256–1264. 10.2337/diabetes.52.5.1256. [PubMed: 12716761]
55. Crosby L, Davis B, Joshi S, Jardine M, Paul J, Neola M, and Barnard ND (2021). Ketogenic Diets and Chronic Disease: Weighing the Benefits Against the Risks. Front Nutr 8, 702802. 10.3389/fnut.2021.702802. [PubMed: 34336911]
56. Song Y, Yang Y, Zeng W, Loor JJ, Jiang Q, Peng Z, Li Y, Jiang S, Feng X, Du X, et al. (2022). beta-Hydroxybutyrate impairs neutrophil migration distance through activation of a protein kinase C and myosin light chain 2 signaling pathway in ketotic cows. J Dairy Sci 105, 761–771. 10.3168/jds.2021-20875. [PubMed: 34635355]
57. Dong Z, Sun X, Tang Y, Luo S, Jia H, Xu Q, Jiang Q, Loor JJ, Xu W, and Xu C (2022). beta-hydroxybutyrate impairs monocyte function via the ROS-NLR family pyrin domain-containing three inflammasome (NLRP3) pathway in ketotic cows. Front Vet Sci 9, 925900. 10.3389/fvets.2022.925900. [PubMed: 36105004]

58. Wang A, Huen SC, Luan HH, Yu S, Zhang C, Gallezot JD, Booth CJ, and Medzhitov R (2016). Opposing Effects of Fasting Metabolism on Tissue Tolerance in Bacterial and Viral Inflammation. Cell 166, 1512–1525 e1512. 10.1016/j.cell.2016.07.026. [PubMed: 27610573]
59. Kadurugamuwa JL, and Beveridge TJ (1995). Virulence factors are released from Pseudomonas aeruginosa in association with membrane vesicles during normal growth and exposure to gentamicin: a novel mechanism of enzyme secretion. J Bacteriol 177, 3998–4008. 10.1128/jb.177.14.3998-4008.1995. [PubMed: 7608073]
60. Ellis TN, Leiman SA, and Kuehn MJ (2010). Naturally produced outer membrane vesicles from Pseudomonas aeruginosa elicit a potent innate immune response via combined sensing of both lipopolysaccharide and protein components. Infect Immun 78, 3822–3831. 10.1128/IAI.00433-10. [PubMed: 20605984]
61. Vanaja SK, Russo AJ, Behl B, Banerjee I, Yankova M, Deshmukh SD, and Rathinam VAK (2016). Bacterial Outer Membrane Vesicles Mediate Cytosolic Localization of LPS and Caspase-11 Activation. Cell 165, 1106–1119. 10.1016/j.cell.2016.04.015. [PubMed: 27156449]
62. McElvaney OJ, Zaslona Z, Becker-Flegler K, Palsson-McDermott EM, Boland F, Gunaratnam C, Gulbins E, O'Neill LA, Reeves EP, and McElvaney NG (2019). Specific Inhibition of the NLRP3 Inflammasome as an Antiinflammatory Strategy in Cystic Fibrosis. Am J Respir Crit Care Med 200, 1381–1391. 10.1164/rccm.201905-1013OC. [PubMed: 31454256]
63. del Campo R, Martinez E, del Fresno C, Alenda R, Gomez-Pina V, Fernandez-Ruiz I, Siliceo M, Jurado T, Toledano V, Arnalich F, et al. (2011). Translocated LPS might cause endotoxin tolerance in circulating monocytes of cystic fibrosis patients. PLoS One 6, e29577. 10.1371/journal.pone.0029577. [PubMed: 22216320]
64. King JD, Kocincova D, Westman EL, and Lam JS (2009). Review: Lipopolysaccharide biosynthesis in Pseudomonas aeruginosa. Innate Immun 15, 261–312. 10.1177/1753425909106436. [PubMed: 19710102]
65. Nowicki EM, O'Brien JP, Brodbelt JS, and Trent MS (2014). Characterization of Pseudomonas aeruginosa LpxT reveals dual positional lipid A kinase activity and coordinated control of outer membrane modification. Mol Microbiol 94, 728–741. 10.1111/mmi.12796. [PubMed: 25223756]
66. Weiss JM, Davies LC, Karwan M, Ileva L, Ozaki MK, Cheng RYS, Ridnour LA, Annunziata CM, Wink DA, and McVicar DW (2018). Itaconic acid mediates crosstalk between macrophage metabolism and peritoneal tumors. Journal of Clinical Investigation 128, 3794–3805. 10.1172/jci99169. [PubMed: 29920191]
67. Bambouskova M, Potuckova L, Paulenda T, Kerndl M, Mogilenko DA, Lizotte K, Swain A, Hayes S, Sheldon RD, Kim H, et al. (2021). Itaconate confers tolerance to late NLRP3 inflammasome activation. Cell Rep 34, 108756. 10.1016/j.celrep.2021.108756. [PubMed: 33691097]
68. Lampropoulou V, Sergushichev A, Bambouskova M, Nair S, Vincent EE, Loginicheva E, Cervantes-Barragan L, Ma X, Huang SC, Griss T, et al. (2016). Itaconate Links Inhibition of Succinate Dehydrogenase with Macrophage Metabolic Remodeling and Regulation of Inflammation. Cell Metab 24, 158–166. 10.1016/j.cmet.2016.06.004. [PubMed: 27374498]
69. O'Neill LAJ, and Artyomov MN (2019). Itaconate: the poster child of metabolic reprogramming in macrophage function. Nat Rev Immunol 19, 273–281. 10.1038/s41577-019-0128-5. [PubMed: 30705422]
70. Peace CG, and O'Neill LA (2022). The role of itaconate in host defense and inflammation. J Clin Invest 132. 10.1172/JCI148548.
71. Asif S, Kim RY, Fatica T, Sim J, Zhao X, Oh Y, Denoncourt A, Cheung AC, Downey M, Mulvihill EE, and Kim KH (2022). Hmgcs2-mediated ketogenesis modulates high-fat diet-induced hepatosteatosis. Mol Metab 61, 101494. 10.1016/j.molmet.2022.101494. [PubMed: 35421611]
72. Badman MK, Pissios P, Kennedy AR, Koukos G, Flier JS, and Maratos-Flier E (2007). Hepatic fibroblast growth factor 21 is regulated by PPARalpha and is a key mediator of hepatic lipid metabolism in ketotic states. Cell Metab 5, 426–437. 10.1016/j.cmet.2007.05.002. [PubMed: 17550778]
73. Badman MK, Koester A, Flier JS, Kharitonenkov A, and Maratos-Flier E (2009). Fibroblast growth factor 21-deficient mice demonstrate impaired adaptation to ketosis. Endocrinology 150, 4931–4940. 10.1210/en.2009-0532. [PubMed: 19819944]

74. Youm YH, Nguyen KY, Grant RW, Goldberg EL, Bodogai M, Kim D, D'Agostino D, Planavsky N, Lupfer C, Kanneganti TD, et al. (2015). The ketone metabolite beta-hydroxybutyrate blocks NLRP3 inflammasome-mediated inflammatory disease. Nat Med 21, 263–269. 10.1038/nm.3804. [PubMed: 25686106]

75. Graff EC, Fang H, Wanders D, and Judd RL (2016). Anti-inflammatory effects of the hydroxycarboxylic acid receptor 2. Metabolism 65, 102–113. 10.1016/j.metabol.2015.10.001. [PubMed: 26773933]

76. Karagiannis F, Peukert K, Surace L, Michla M, Nikolka F, Fox M, Weiss P, Feuerborn C, Maier P, Schulz S, et al. (2022). Impaired ketogenesis ties metabolism to T cell dysfunction in COVID-19. Nature 609, 801–807. 10.1038/s41586-022-05128-8. [PubMed: 35901960]

77. Armeni E, Aziz U, Qamar S, Nasir S, Nethaji C, Negus R, Murch N, Beynon HC, Bouloux P, Rosenthal M, et al. (2020). Protracted ketonaemia in hyperglycaemic emergencies in COVID-19: a retrospective case series. Lancet Diabetes Endocrinol 8, 660–663. 10.1016/S2213-8587(20)30221-7. [PubMed: 32621809]

78. Kanikarla-Marie P, and Jain SK (2016). Hyperketonemia and ketosis increase the risk of complications in type 1 diabetes. Free Radic Biol Med 95, 268–277. 10.1016/j.freeradbiomed.2016.03.020. [PubMed: 27036365]

79. Elsheikh M, and Conway GS (1998). The impact of obesity on cardiovascular risk factors in Turner's syndrome. Clin Endocrinol (Oxf) 49, 447–450. 10.1046/j.1365-2265.1998.00552.x. [PubMed: 9876341]

80. Martinez-Outschoorn UE, Peiris-Pages M, Pestell RG, Sotgia F, and Lisanti MP (2017). Cancer metabolism: a therapeutic perspective. Nat Rev Clin Oncol 14, 113. 10.1038/nrclinonc.2017.1.

81. Martinez-Outschoorn UE, Lin Z, Whitaker-Menezes D, Howell A, Sotgia F, and Lisanti MP (2012). Ketone body utilization drives tumor growth and metastasis. Cell Cycle 11, 3964–3971. 10.4161/cc.22137. [PubMed: 23082722]

82. Ogger PP, Albers GJ, Hewitt RJ, O'Sullivan BJ, Powell JE, Calamita E, Ghai P, Walker SA, McErlean P, Saunders P, et al. (2020). Itaconate controls the severity of pulmonary fibrosis. Sci Immunol 5. 10.1126/sciimmunol.abc1884.

Highlights

- *P. aeruginosa* surface LPS interferes airway cell ATP synthase function.
- This bioenergetic impairment triggers detrimental inflammation and alveolar damage.
- The host responds to ATP synthase inhibition by *P. aeruginosa* via ketogenesis.
- Ketone bodies repress *P. aeruginosa* LPS assembly, limiting damaging inflammation.

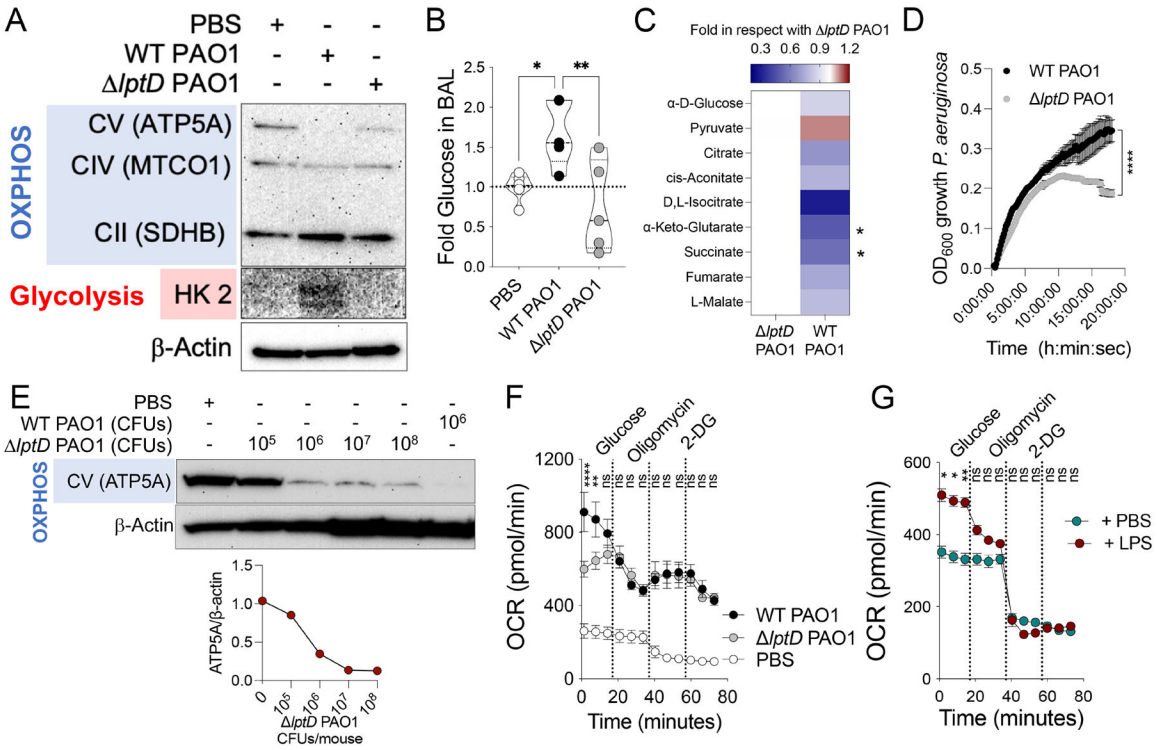

Figure 1. ***P. aeruginosa*** **LPS display inhibits pulmonary ATP synthase –**

Mice were treated with PBS, WT PAO1, or *ΔlptD* PAO1. The following was measured: **A**) OXPHOS (ATP5A, MTCO1, SDHB) and glycolysis (HK2) in lung; **B**) BAL glucose. **C**) NADH and $FADH_2$ abundance in WT and *ΔlptD* PAO1 via Biolog plates. **D**) WT and *ΔlptD* PAO1 growth in succinate-rich minimal media. **E**) Lung ATP5A expression in mice exposed to either PBS, WT PAO1, or *ΔlptD* PAO1. ATP5/β-actin ratio is shown. **F-G**) BDMDs oxygen consumption rate (OCR). Data are shown as average of 2-3 independent experiments +/− SEM. B-C: t-Student test. D, F-G: Two-Way ANOVA. *: $P<0.05$; **: $P<0.01$; ****: $P<0.0001$; ns: non-significant.

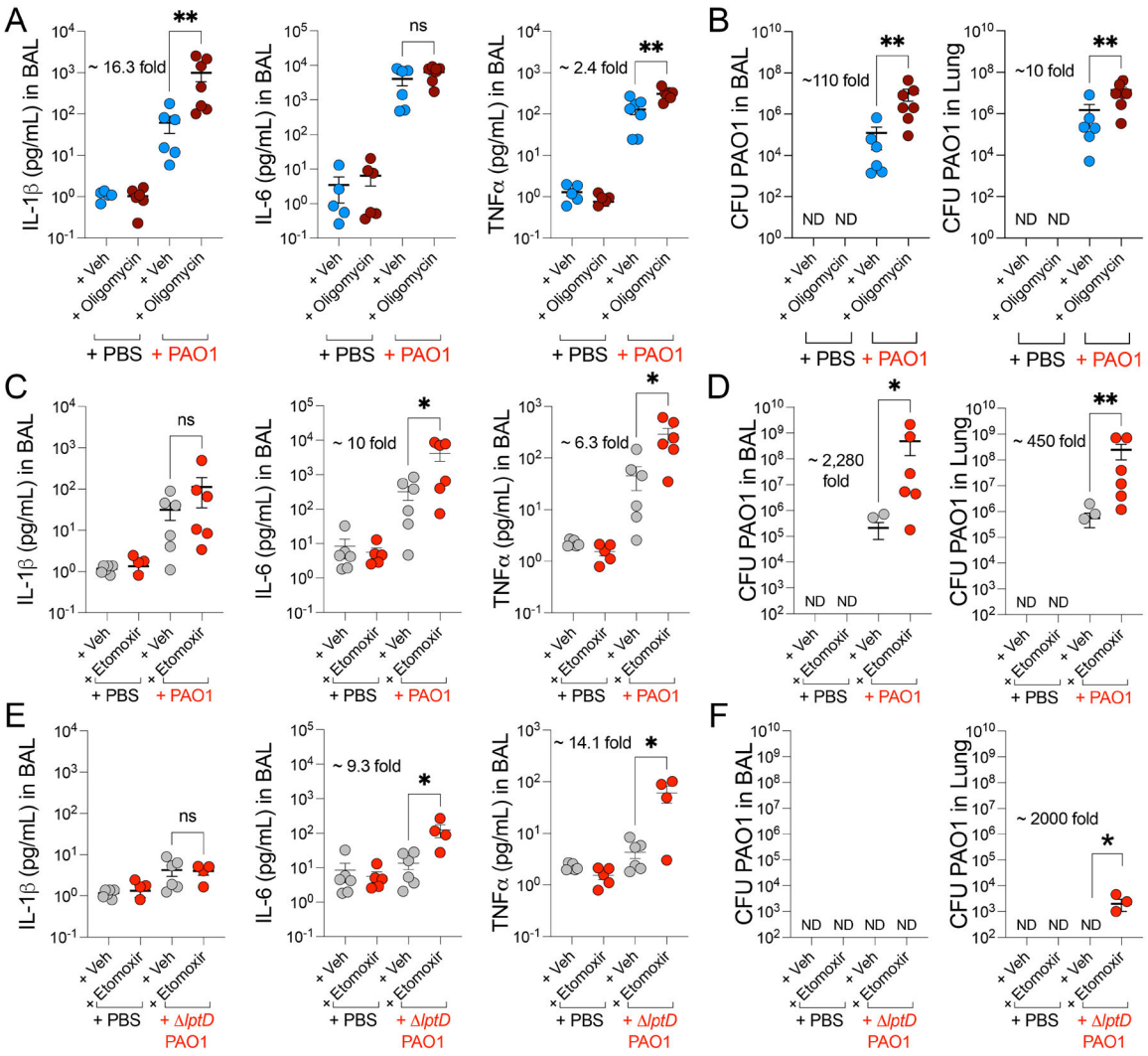

Figure 2. Host OXPHOS impairment worsens lung inflammation and *P. aeruginosa* burden – Mice were administered either vehicle or oligomycin (ATP synthase inhibitor) and exposed to PBS or WT PAO1. The following were analyzed: **A**) BAL cytokines; **B**) bacterial burden in BAL and lung. Animals were treated with either vehicle or etomoxir (FAO blocker) and exposed to PBS, WT PAO1, or *ΔlptD* PAO1. The following were examined: **C**) BAL cytokines for WT PAO1; **D**) bacterial burden in BAL and lung for WT PAO1; **E**) BAL cytokines for *ΔlptD* PAO1; **F**) bacterial burden in BAL and lung for *ΔlptD* PAO1. Data are shown as average of 2-3 independent experiments +/− SEM, 4-7 mice in total. A-F: One-Way ANOVA. *: $P<0.05$; **: $P<0.01$; ns: non-significant. See also Figure S1.

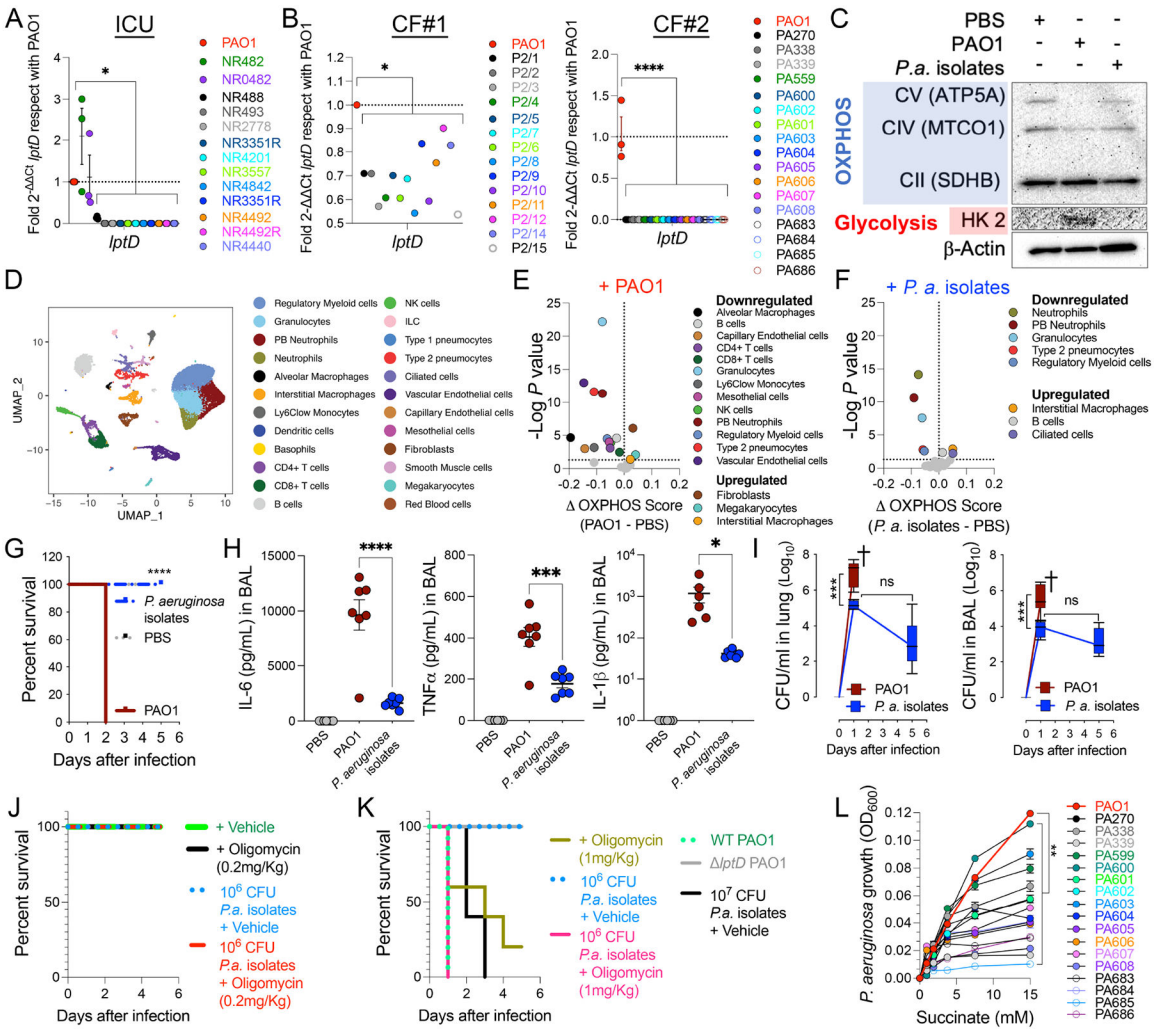

Figure 3. *P. aeruginosa* isolates preserve airway OXPHOS and enable host-pathogen coexistence

–

LptD mRNA levels in *P. aeruginosa* strains from: **A**) 13 patients at ICU; **B**) tolerant people with CF: CF#1: 14 strains; CF#2: 17 strains. Animals were exposed to PBS, WT PAO1, or a mixture of the 17 *P. aeruginosa* isolates from CF#2. The following were analyzed: **C**) OXPHOS (ATP5A, MTCO1, SDHB) and glycolysis (HK2) in lung; **D**) pulmonary cell subsets identified by scRNA-Seq; **E-F**) ΔOXPHOS transcriptomic score per lung population in response to each pathogen; **G**) mouse survival; **H**) BAL cytokines; **I**) bacterial burden in lung and BAL (black cross indicates all animal are dead). **J-K**) Survival of animals exposed to either ~10^6 or ~10^7 CFUs of the *P. aeruginosa* isolates and then treated with either a sublethal (J) or lethal dose (K) of oligomycin. WT and *ΔlptD* PAO1 were also studied. **L**) Bacterial endpoint growth in increasing succinate. Data are shown as average +/− SEM. C-I: 2-3 independent experiments, with 3-7 animals in total. J-K: 2 independent experiments, with 5 mice in total. I, L: Two-Way ANOVA; G, J-K: Kaplan-Maier; H: One-Way ANOVA. *: P<0.05; **: P<0.01; ***: P<0.001; ****: P<0.0001; ns: non-significant. See also Figure S1, Figure S2, Table S1 and Table S2.

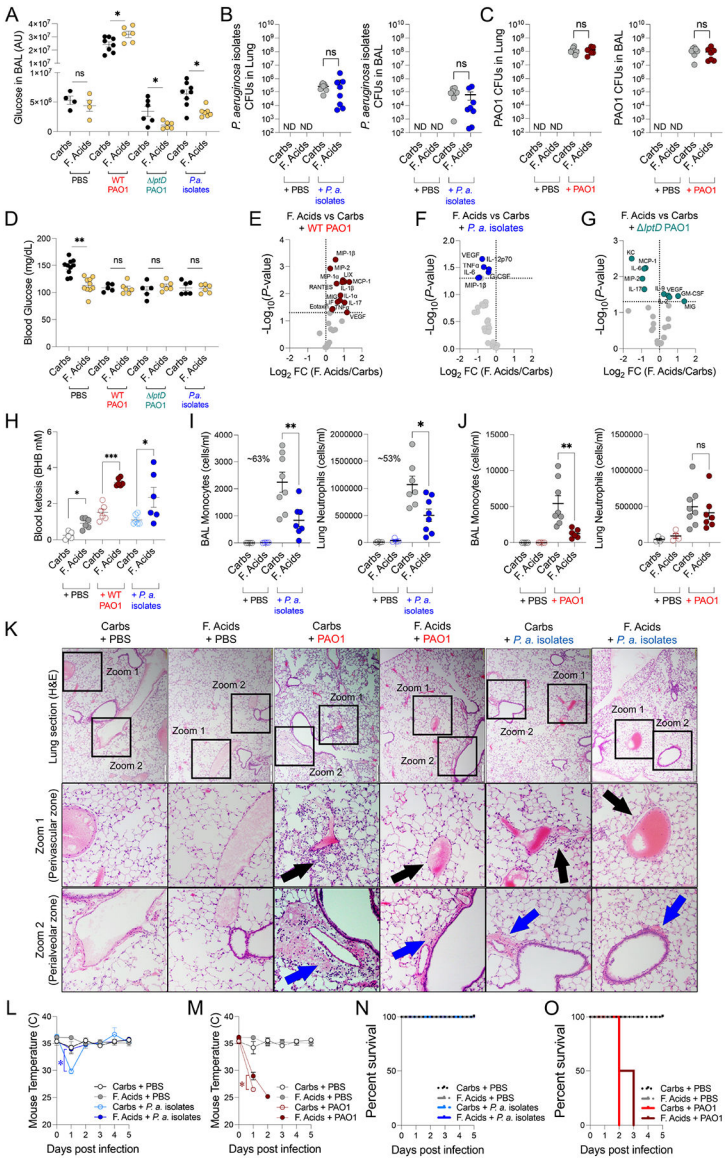

Figure 4. Dietary fats modulate host tolerance to *P. aeruginosa* lung infection –

Mice fed with either a fatty acid-rich (F. Acids) or a carbohydrate-rich (Carbs) diet were exposed to PBS, WT PAO1, *ΔlptD* PAO1 or the *P. aeruginosa* isolates. The following were examined: **A**) BAL glucose; **B-C**) bacterial burden; **D**) glycemia; **E-G**) BAL cytokines enrichment; **H**) blood BHB (beginning of the light cycle); **I-J**) phagocyte recruitment in BAL and lung; **K**) Lung H&E; **L-M**) body temperature; **N-O**) animal survival; Data are from 2-3 independent assays, 4-8 mice in total, and shown as average +/− SEM. A-D, H-J: One-Way ANOVA. L-M: Two-Way ANOVA. N-O: Kaplan-Maier. E-G: t-Student test. *: $P<0.05$; **: $P<0.01$; ***: $P<0.001$; ns: non-significant. See also Figure S3.

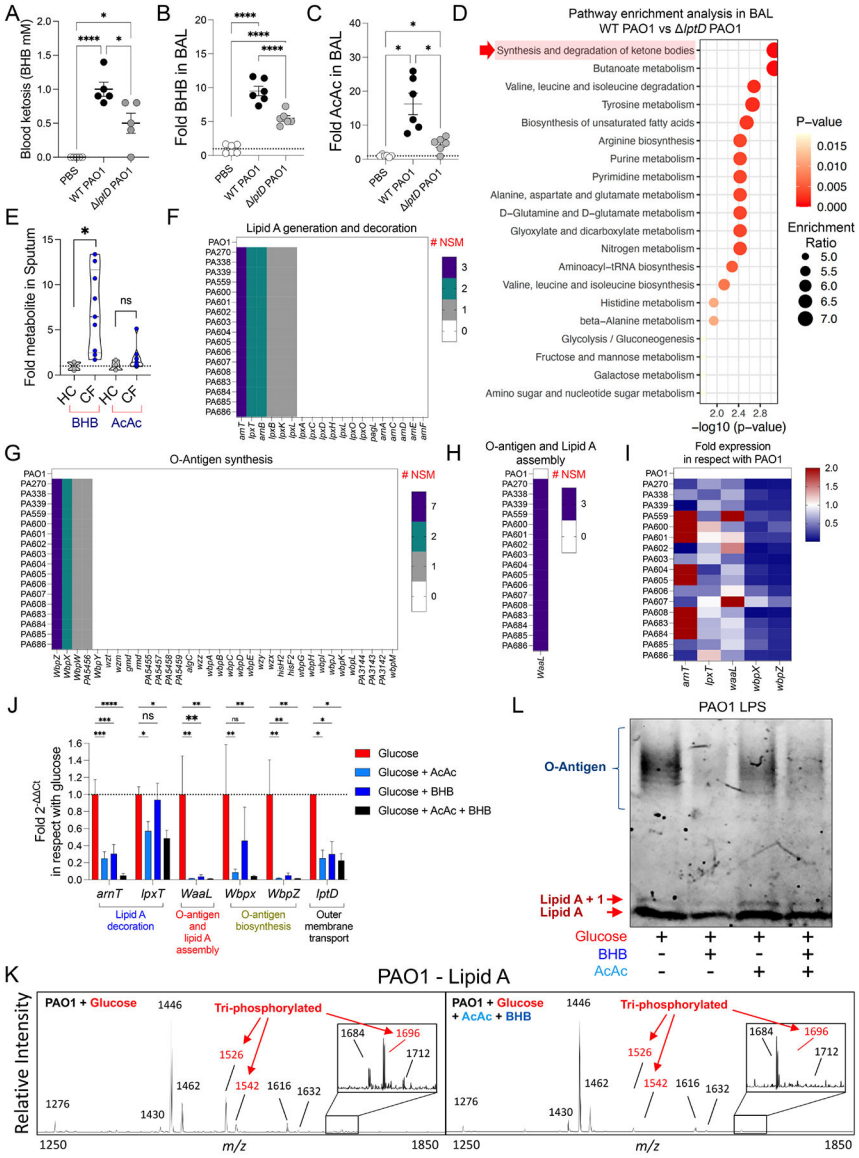

Figure 5. Airway ketones drive *P. aeruginosa* LPS patho-adaptation –

Mice were exposed to PBS, WT PAO1, or *ΔlptD* PAO1. The following were measured at the beginning of the light cycle: **A**) BHB in blood; **B-D**) BHB and AcAc abundance in BAL. In D, pathway enrichment analysis was performed via Metaboloanalyst 5.0 using the KEGG platform as database. **E**) Ketones in sputum of HC and individuals with CF. **F-H**) Number of non-synonymous mutations (NSM) found in each *P. aeruginosa* isolate in routes linked to LPS biogenesis. **I**) mRNA levels of LPS assembly genes. WT PAO1 was grown in glucose-rich minimal media and complemented with AcAc, BHB, or both ketones. The following were measured: **J**) mRNA levels of gene clusters involved in LPS assembly; **K**) lipid A phosphorylation via MALDI-TOF; **L**) O-antigen abundance. Data are shown as average +/− SEM from 2-3 independent assays. A-D: 5-6 mice in total per group. A-C, J: One-Way ANOVA. D-E: t-Student test: *: $P<0.05$; **: $P<0.01$; ***: $P<0.001$; ****: $P<0.0001$; ns: non-significant. See also Figure S4.

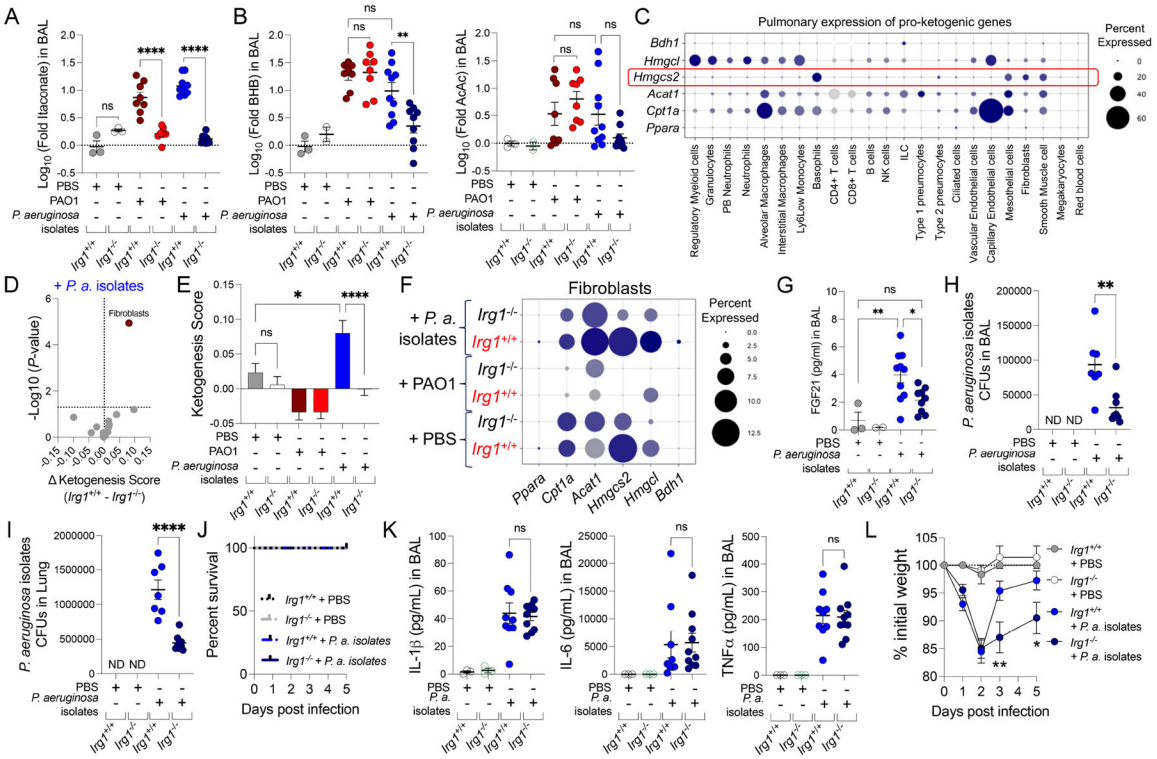

Figure 6. Itaconate promotes ketone enrichment in the lung during *P. aeruginosa* infection –

Irg1$^{+/+}$ and *Irg1*$^{-/-}$ mice were exposed to PBS, WT PAO1, or the *P. aeruginosa* isolates. The following were measured: **A-B**) BAL metabolites; **C**) mRNA expression of ketogenic clusters in each lung cell subset identified by scRNA-Seq; **D**) Volcano plot of Δketogenesis scores ("*Irg1*$^{+/+}$" – "*Irg1*$^{-/-}$") for each lung cell subset during infection with the *P. aeruginosa* isolates; **E**) ketogenesis transcriptomic score in fibroblasts; **F**) Expression of ketogenic clusters in fibroblasts; **G**) BAL FGF21; **H-I**) respiratory pathogen burden during infection with the *P. aeruginosa* isolates; **J**) animal survival; **K**) BAL cytokines; **L**) weight change. Data are shown as average +/− SEM from 2-3 independent experiments, with 3-10 animals in total. A-B, E, G-I: One-Way ANOVA; L: Two-Way ANOVA; D: t-Student test. J: Kaplan-Maier. *: P<0.05; **: P<0.01; ***: P<0.001; ****: P<0.0001; ns: non-significant. See also Figure S5, Figure S6, and Table S2.

KEY RESOURCES TABLE

REAGENT or RESOURCE	SOURCE	IDENTIFIER
Antibodies		
Anti-mouse CD45 AF700	Biolegend	Cat 103128, RRID:AB_493715
Anti-mouse CD11c Bv605	Biolegend	Cat 117333, RRID:AB_11204262
Anti-mouse SiglecF	Biolegend	Cat 562680, RRID:AB_2687570
Anti-mouse CD11b AF594	Biolegend	Cat 101254, RRID:AB_2563231
Anti-mouse MHC II APC/Cy7	Biolegend	Cat 107628, RRID:AB_2069377
Anti-mouse Ly6C Bv421	Biolegend	Cat 128032, RRID:AB_2562178
Anti-mouse Ly6G PerCP/Cy5.5	Biolegend	Cat 127616, RRID:AB_1877271
anti-β-actin	Sigma	Cat A5441, RRID:AB_476744
OXPHOS rodent WB antibody cocktail	Thermo Fisher Scientific	Cat 45-8099, RRID:AB_2533835
hexokinase 2 polyclonal antibody	Thermo Fisher Scientific	Cat 22029-1-AP, RRID:AB_11182717
Goat anti-Ms IgG HRP	Santa Cruz	Cat sc-2005, RRID:AB_631736
Goat anti-Rb IgG HRP	Santa Cruz	Cat sc-2004, RRID:AB_631746
Biological Samples		
CF sputum samples	This Study	N/A
Chemicals, peptides, and recombinant proteins		
Oligomycin	Selleckchem	S1478
Etomoxir	Sigma Aldrich	E1905
Succinic acid	Sigma Aldrich	14160
D-Glucose	Sigma Aldrich	G8270
Trizol™ Reagent	Thermo Fisher Scientific	15596026
Novex™ 10-20% Tricine Protein Gels	Thermo Fisher Scientific	EC6625BOX
Pro-Q™ Emerald 300 Lipopolysaccharide Gel Stain Kit	Thermo Fisher Scientific	P20495
Live/Dead DAPi dye	Thermo Fisher Scientific	Cat L34962
Formalin free tissue fixative	Sigma Aldrich	Cat A5472
Paraformaldehyde 32%	Electron Microscopy Sciences	Cat 15714-S
Methanol	Thermo Fisher Scientific	Cat A456-1
Methanol	Alpha Aesar	Cat 22909
Trypan blue stain	Invitrogen	Cat T10282
Glucose	Agilent	Cat 103577-100
collagenase I	Gibco	1100-017
Elastase	Worthington	LS006365
Dispase	Gibco	17105-041
BSA	Thermo Fisher Scientific	BP9705
Critical Commercial Assays		
Mouse Cytokine Array / Chemokine Array 31-Plex	Evetechnologies	MD31
Seahorse XFe24 FluxPaks	Agilent Technologies	102340-100

REAGENT or RESOURCE	SOURCE	IDENTIFIER
RNeasy Mini Kit	Qiagen	Cat 74104
E.Z.N.A.® Total RNA Kit I	Omega Biotek	R6834-01
DNA free removal kit	Thermo Fisher Scientific	AM1906
High-Capacity cDNA Reverse Transcription Kit	Applied Biosystems	4368813
Power SYBR™ Green PCR Master Mix	Applied Biosystems	4368577
Biolog MitoPlate S-1	Biolog	Cat 14105
Biolog Redox Dye Mix MC	Biolog	Cat 74353
Experimental Models: Organisms/Strains		
Mouse: C57BL/6	Jackson Laboratories	JAX: 000664
Mouse: C57BL/6J/N	Jackson Laboratories	JAX: 005304
Mouse: C57BL/6 *Irg1*$^{-/-}$*(Acod1*$^{-/-}$*)*	Jackson Laboratories	JAX: 029340
Mouse: B6.129S7-Il1r1tm1Imx/J (*Il1r*$^{-/-}$)	Jackson Laboratories	JAX: 003245
Bacterial and Virus Strains		
P. aeruginosa WT PAO1	Our laboratory	N/A
P. aeruginosa WT PAO1	Provided by Dr. CJ Balibar; Balibar et al, 2015	N/A
P. aeruginosa Δ*lptD* PAO1 (mutant 4213)	Provided by Dr. CJ Balibar; Balibar et al, 2015	N/A
CF subject 2 *P. aeruginosa* isolates	Riquelme et al, 2019	N/A
CF subject 1 *P. aeruginosa* isolates	Provided by Dr. Barbara Kahl	N/A
ICU *P. aeruginosa* isolates	Provided by Dr. A.C. Uhlemman	N/A
Oligonucleotides		
rpsL-F: CGGCACTGCGTAAGGTATGC	Riquelme et al. 2019	N/A
rpsL-R: CGTACTTCGAACGACCCTGCT	Riquelme et al. 2019	N/A
lptD-F: CCTGCCCTACAACCCAGGTG	Riquelme et al. 2019	N/A
lptD-R: ATGCTGCCGTCGTCATTGAA	Riquelme et al. 2019	N/A
waaL-F: CTACGCCAGATCAGCGAGCA	Riquelme et al. 2019	N/A
waaL-R: CCTCCAGCGAAAAGCACACC	Riquelme et al. 2019	N/A
wbpX-F: GAGACCATCCGCGACGAAGT	Riquelme et al. 2019	N/A
wbpX-R: TCCTCCACCAGGTCCAGCTC	Riquelme et al. 2019	N/A
wbpZ-F: GCTCCGCCAGTACCGAGAAA	Riquelme et al. 2019	N/A
wbpZ-R: ATCACCCCGACGAACAGGAA	Riquelme et al. 2019	N/A
lpxT-F: CTGACCTTCGGCTTCATCGT	Nowicki et al. 2014	N/A
lpxT-R: TGGAGCGGTCCTTGATTTCC	Nowicki et al. 2014	N/A
arnT-F: GGCTATGCCAACCTCGACCC	Nowicki et al. 2014	N/A
arnT-R: GCGAGGAAGCCCTTGGTCAG	Nowicki et al. 2014	N/A
Software and Algorithms		
GraphPad Prism 9	GraphPad Software	https://www.graphpad.com
FlowJo X Flow cytometry	FlowJo	https://www.flowjo.com
FIJI	FIJI	http://imagej.net

REAGENT or RESOURCE	SOURCE	IDENTIFIER
Seurat v4, Seurat v5	Seurat library	https://satijalab.org
MetaboloAnalyst 5.0	MetaboloAnalyst	https://www.metaboanalyst.ca
Kyoto Encyclopedia of Genes and Genomes	KEGG	https://www.genome.jp/kegg/
Adobe Photoshop 24.5.0	Adobe	https://www.adobe.com/
Deposited data		
scRNA-Seq lung tissue	GEO	Access number: GSE203352
Raw metabolomics BAL tissue	MetaboLights	Access numbers: MTBLS4922, MTBLS4923, and MTBLS4924
P. aeruginosa isolates genomes	NIH SRA	Access numbers: PA270 (SRR8775051), PA338 (SRR8775050), PA339 (SRR8775058), PA599 (SRR8775057), PA600 (SRR8775065), PA601 (SRR8775054), PA602 (SRR8775055), PA603 (SRR8775053), PA604 (SRR8775056), PA605 (SRR8775052), PA606 (SRR8775060), PA607 (SRR8775059), PA608 (SRR8775062), PA683 (SRR8775061), PA684 (SRR8775064), PA685 (SRR8775063) and PA686 (SRR8775066).
Raw Data	Data S1	
Other		
RPMI 1640 1x with glutamine	Corning	10-040-CV
Antibiotic Penicillin-Streptomycin	Corning	30-002-CI
Fetal Bovine Serum	Gibco	26140-079
KetoBM Ketone Strips	KBM	ASIN: B087JYC6JD
KetoBM Blood Ketone Meter Kit for Keto Diet Testing	KetoBM	ASIN: B07QWMM4M6
AUVON I-QARE DS-W Draw-in Blood Glucose Test Strips	AUVON	ASIN: B09T6CHZVZ
AUVON DS-W Diabetes Sugar Testing Meter	AUVON	ASIN: B081ZY1LHV
Irradiated Fatty Acid rich diet	Research Diets, Inc	D10070801i
Irradiated Carbohydrate rich diet	Research Diets, Inc	D19082304i
Irradiated Purina regular chow	Purina	5053